



**Politecnico  
di Torino**

**POLITECNICO DI TORINO**

**Master's Degree in Biomedical Engineering  
A.a 2022/2023  
Master's Degree Thesis**

**Development of extracellular  
vesicle-encapsulated nanoparticles as a  
biomimetic nucleic acid vaccine**

**Supervisors**

**Prof. VALENTINA ALICE CAUDA**

**Prof. SALVADOR BORROS**

**Prof. CRISTINA FORNAGUERA**

**Candidate**

**ALESSANDRO MASOERO**



## Abstract

Current cancer therapies are limited by several side effects, especially when talking about chemotherapy and radiotherapy, or the impossibility of eradicate the tumor. In recent years, immunotherapies have been proposed both as an alternative and as a complementary solution to these problems. Immunotherapy finds groundwork in the already present tumor-controlling mechanisms adopted by the immune system; however, tumors have evolved around these machineries in several ways. The result is the need to boost the immune system in order to overcome the immunosuppression and immunoevasion mechanisms. Cancer vaccines can in principle solve this problem by delivering antigen-encoding nucleic acids to antigen-presenting cells, which will elicit an antigen-specific CD8+ cytotoxic T lymphocytes mediated response. Nucleic acid delivery brings many challenges, for example, the preservation of the genetic material from enzymatic degradation and the need for cell-specific and targeted internalization. Polymeric nanoparticles and synthetic lipid vesicles have shown great success transfecting cells *in vitro* but they lack targeting abilities when applied *in vivo*. Poly(beta-amino esters) have been able to serve as gene delivery vectors, thanks to their many advantages such as the cationic surface charge, the endosomal escape, or the biocompatibility, but they have shown unspecific biodistribution *in vivo*. On the other hand, natural tropism showed by certain extracellular vesicles is a promising feature to be applied in nanomedicine. In the case of immune cells, extracellular vesicles have shown a preferential uptake in cells of the same nature as the parental cell, opening the possibility to exploit these vesicles as a functional active targeting moiety. Here I present for the first time the combination of pBAEs nanoparticles with extracellular vesicle-coating. The encapsulation was performed by applying freeze-thaw cycles to EVs and then incubating them with pBAEs NPs at room temperature in order to let the membrane fusion encapsulation. The EV-encapsulated NPs were then characterized in terms of their hydrodynamic size and concentration and analyzed by confocal microscopy and hyperspectral microscopy to assess the colocalization of the polymer and the lipid bilayer. Finally, the uptake was evaluated by *in vitro* internalization assay both with flow cytometry and confocal microscopy with fixed cells, demonstrating that EV-encapsulated NPs can effectively enter the cells with the same or higher efficacy and efficiency if compared to the naked pBAE NPs. Thus, it can be concluded that pBAEs NPs were successfully encapsulated and, moreover, this biomimetic coating enhanced properly the *in vitro* cellular uptake of the nanoparticles.

## Riassunto

Le attuali terapie contro il cancro sono limitate da diversi effetti collaterali, specialmente nel caso di chemioterapia e radioterapia, o dall'impossibilità di eradicare completamente il tumore. Negli ultimi anni, le immunoterapie sono state proposte come alternativa e soluzione complementare a questi problemi. Le immunoterapie si basano sui meccanismi di controllo tumorale già presenti nel sistema immunitario; tuttavia, i tumori si sono evoluti attorno a tali meccanismi in vari modi. Vi è la necessità di potenziare il sistema immunitario per superare i meccanismi di immunosoppressione e immunoevasione. Le vaccinazioni contro il cancro possono in teoria risolvere questo problema mediante la consegna di acidi nucleici codificanti antigeni alle cellule APC (antigen-presenting cell), stimolando una risposta mediata dai linfociti T citotossici CD8+ specifica per l'antigene. La consegna di acidi nucleici presenta molte sfide, come la preservazione del materiale genetico dalla degradazione enzimatica e la necessità di internalizzazione mirata e specifica per le cellule. Le nanoparticelle polimeriche e le vescicole sintetiche lipidiche hanno dimostrato un grande successo nella trasfezione delle cellule in vitro, ma mancano di capacità di targeting quando vengono applicate in vivo. I poli( $\beta$ -amino esteri) (pBAEs) sono stati in grado di servire come gene vector, grazie ai loro numerosi vantaggi, come la carica superficiale cationica, l'endosomal escape o la biocompatibilità, ma hanno mostrato una biodistribuzione non specifica in vivo. D'altra parte, il tropismo naturale mostrato da alcune vescicole extracellulari rappresenta una caratteristica promettente da applicare in nanomedicina. Nel caso delle cellule del sistema immunitario, le vescicole extracellulari hanno dimostrato di essere preferenzialmente internalizzate dalle cellule della stessa natura della cellula madre, aprendo la possibilità di sfruttare queste vescicole per un re-targeting attivo funzionale. Qui presento per la prima volta la combinazione di nanoparticelle di pBAEs con il rivestimento di vescicole extracellulari. L'incapsulamento è stato eseguito applicando cicli di congelamento-scongelo alle vescicole extracellulari e poi incubandole con nanoparticelle di pBAEs a temperatura ambiente per consentire l'incapsulamento mediante fusione della membrana. Le nanoparticelle incapsulate nelle vescicole sono state quindi caratterizzate in termini di diametro idrodinamico e concentrazione e analizzate mediante microscopia confocale e microscopia iperspettrale per valutare la colocalizzazione del polimero e il doppio strato lipidico. Infine, l'assorbimento è stato valutato tramite un test di internalizzazione in vitro, sia con citometria a flusso che con microscopia confocale su cellule fissate, dimostrando che le nanoparticelle incapsulate nelle vescicole possono entrare efficacemente nelle cellule con la stessa o maggiore efficacia ed efficienza rispetto alle nanoparticelle di pBAEs nude. Pertanto, si può concludere che le nanoparticelle di pBAEs sono state incapsulate con successo e, inoltre, questo rivestimento biomimetico ha migliorato adeguatamente l'assorbimento cellulare in vitro delle nanoparticelle.

## Graphical abstract

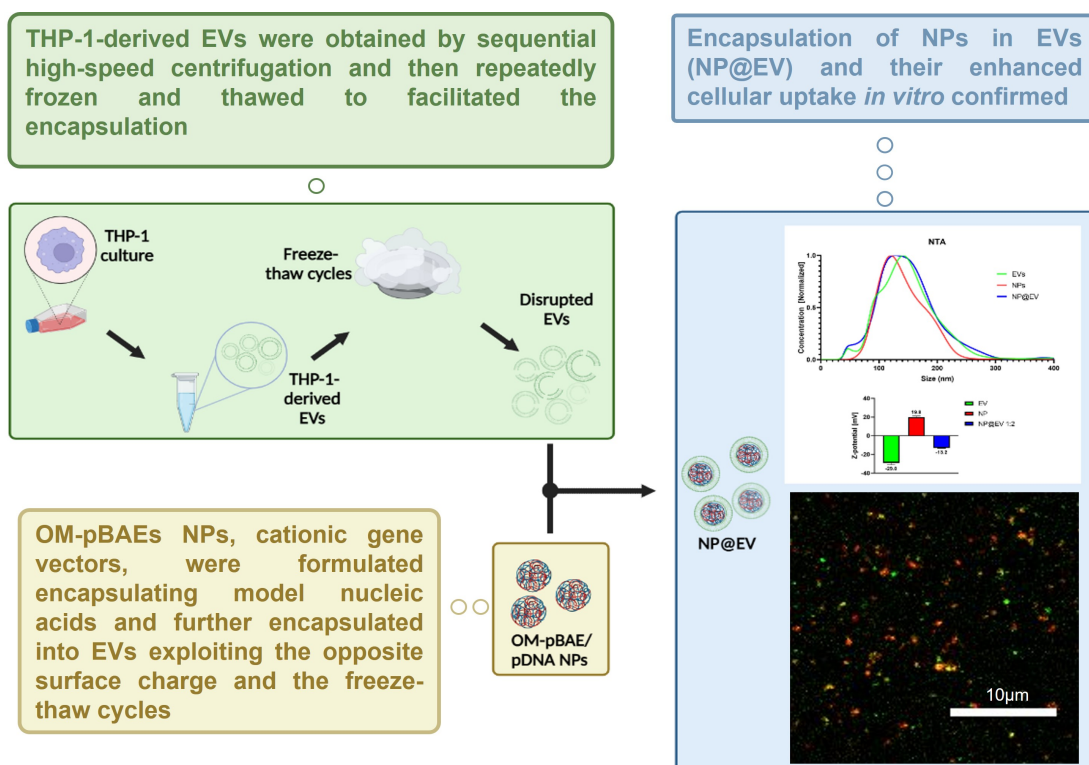


**Figure 1:** The encapsulation process is hereby summarized. THP-1-derived EVs were repeatedly frozen and thawed before being incubated with OM-pBAE NPs. The final characterization by DLS and the colocalization of polymer and lipid bilayer, along with the enhanced cellular uptake *in vitro* have confirmed the successful encapsulation.



## RINGRAZIAMENTI

La lista di persone che vorrei ringraziare potrebbe essere troppo lunga e dovrebbe essere aggiornata di giorno in giorno; chiedo scusa a chi non riuscirò ad inserire in queste poche righe.

Vorrei ringraziare innanzitutto la mia relatrice, la professoressa Valentina Cauda, per avermi scelto per questo fantastico progetto che mi ha permesso di fare un'esperienza inestimabile. Allo stesso modo, ringrazio il professor Salvador Bòrros e la professoressa Cristina Fornaguera per avermi accolto nei loro laboratori dell'Institut Quimic de Sarrià. Il loro sostegno durante i 6 mesi di lavoro, e successivamente per la stesura della tesi, mi hanno permesso di apprendere tantissimo sul mondo della ricerca.

Ringrazio per intero il gruppo GEMAT, il loro aiuto e i loro insegnamenti sono stati determinanti per tutta la mia crescita professionale e per la realizzazione di questo progetto. In particolar modo, vorrei ringraziare Maria Navalon, Carles, Gloria, Dario e Jordi. Un ringraziamento speciale va alle mie due amiche Laura e Monica, con le quali ho condiviso uno stupendo viaggio e che spero di rivedere al più presto sulla tavola da surf.

Ai miei amici dell'università va un ringraziamento speciale per tutto il tempo trascorso insieme negli ultimi 6 anni. Ringrazio Davide, con il quale ho trascorso la maggior parte di questi anni, per tutte le volte che mi ha ospitato a casa sua. Ringrazio Naomi, Sebastiano, Kevin, Federica, Lorenzo e Peppe per tutti i bei momenti trascorsi insieme. Ringrazio i miei compagni di corso con i quali ho potuto studiare, realizzare lavori di gruppo e che mi hanno sempre passato gli appunti, Valentina ed Elisa.

Alla mia intera famiglia va il ringraziamento più grande, perché hanno reso possibile per me questo percorso senza farmi mai mancare nulla. Ringrazio mamma e papà per avermi sempre sostenuto anche nei momenti difficili; ringrazio mia sorella per essere sempre stata un modello da seguire e mi scuso per non essere sempre stato il fratello premuroso che si merita. Ringrazio con tutto il cuore i nonni, quelli che sono ancora oggi al mio fianco e quelli che ho dovuto salutare con eterno dispiacere.

Gli ultimi ringraziamenti vanno a tutte le persone che ho conosciuto e che mi hanno accompagnato nei sei mesi passati a Barcellona, con le quali ho condiviso un'esperienza indimenticabile. Ringrazio tutta la "Aragang", Sofia, Paulo, Kunal, Kato, Sophia, Diego, Julie, Hirbod e tutti gli altri. In modo speciale, vorrei ringraziare due persone fondamentali per questa esperienza e oltre. Ringrazio Alejandra per la sua amicizia, il suo sostegno, sia in laboratorio che personale, per la forza che mi ha trasmesso e per tutti i saggi consigli che mi ha dedicato. Infine, ringrazio Giulia che, anche se da poco meno di un anno, ha conquistato un posto speciale nella mia vita, per avermi regalato momenti felici e spensieratezza e allo stesso tempo di avermi incoraggiato a migliorare me stesso per tutti questi mesi.

## ACKNOWLEDGMENTS

The list of people I would like to thank could be too long and should be updated day by day. I apologize to those I won't be able to mention in these few lines.

First and foremost, I would like to thank my advisor, Professor Valentina Cauda, for choosing me for this fantastic project, which has allowed me invaluable experience. Similarly, I would like to thank Professor Salvador Bòrros and Professor Cristina Fornaguera for welcoming me into their laboratories at the Institut Quimic de Sarrià. Their support during the 6 months of work, and later for the thesis writing, has allowed me to gain huge knowledge about research.

I am grateful to the entire GEMAT group. Their help and teachings have been instrumental in my professional growth and the realization of this project. I would particularly like to thank Maria Navalon, Carles, Gloria, Dario, and Jordi. A special thanks go to my two friends, Laura and Monica, with whom I shared an amazing trip, and I hope to see them soon again on the surfboard.

A special thank you goes to my university friends for all our time together over the past 6 years. I thank Davide, with whom I have spent most of these years, for all the times he hosted me at his place. I thank Naomi, Sebastiano, Kevin, Federica, Lorenzo, and Peppe for all the great moments we have shared. I thank my classmates with whom I have studied, worked on group projects, and who have always shared their notes with me, Valentina, and Elisa.

My deepest gratitude goes to my entire family because they have made this journey possible for me and have never let me lack anything. I thank my mom and dad for always supporting me, even in difficult times. I thank my sister for always being a role model to follow, and I apologize for not always being the caring brother she deserves. I wholeheartedly thank my grandparents, both those who are still by my side and those whom I had to bid farewell to with eternal regret.

The last thanks go to all the people I have met and who accompanied me during the six months in Barcelona, with whom I shared an unforgettable experience. I thank the entire "Aragang" group, Sofia, Paulo, Kunal, Kato, Sophia, Diego, Julie, Hirbod, and all the others. Especially, I would like to thank two fundamental people for this experience and beyond. I thank Alejandra for her friendship, her support both in the lab and personally, for the strength she has transmitted to me, and for all the wise advice she has given me. Finally, I thank Giulia, who, although it has been less than a year, has earned a special place in my life, for giving me happy moments and lightheartedness, and at the same time, encouraging me to improve myself throughout these months.



# Table of Contents

<b>List of Tables</b>	VII
<b>List of Figures</b>	VIII
<b>1 Motivation and objective</b>	<b>1</b>
1.1 Motivation . . . . .	1
1.2 Objective . . . . .	2
<b>2 Biological Background</b>	<b>3</b>
2.1 Cancer therapies: from surgery to anticancer vaccines . . . . .	3
2.2 OM-pBAEs nanoparticles for nucleic acid delivery . . . . .	7
2.3 Extracellular vesicles: a natural targeting moiety . . . . .	8
<b>3 Materials and methods</b>	<b>11</b>
3.1 Materials . . . . .	11
3.2 Cell Culture . . . . .	12
3.2.1 Differentiation of THP-1 cell line . . . . .	12
3.3 Nanosystems preparation . . . . .	12
3.3.1 Synthesis of OM-pBAE nanoparticles . . . . .	12
3.3.2 Labeling R-pBAE with fluorophore . . . . .	12
3.3.3 Harvesting and purification of Extracellular Vesicles . . . . .	13
3.3.4 Labeling of Extracellular Vesicles . . . . .	13
3.3.5 Sonication and extrusion methods . . . . .	13
3.3.6 Encapsulation method . . . . .	14
3.4 Physicochemical characterization of the nanoformulations an <i>in vitro</i> studies . . . . .	14
3.4.1 Dynamic Light Scattering (DLS) and Nanoparticles Tracking Analysis (NTA) . . . . .	14
3.4.2 Hyperspectral microscopy . . . . .	15
3.4.3 Western Blot . . . . .	15
3.4.4 Flow cytometry . . . . .	16

3.4.5	In vitro transfection study . . . . .	17
3.4.6	Confocal microscopy . . . . .	17
3.5	Statistical analysis . . . . .	17
<b>4</b>	<b>Results and discussion</b>	<b>19</b>
4.1	Methodology of encapsulation set up . . . . .	19
4.2	Characterization of the nanoformulations . . . . .	23
4.2.1	Physicochemical characterization: size, surface charge, poly- dispersity and concentration . . . . .	23
4.2.2	Determining the NP@EV complexation by fluorescent mi- croscopy . . . . .	25
4.2.3	Western Blot analysis to confirm nanostructures are EVs . .	28
4.3	<i>In vitro</i> uptake studies . . . . .	29
4.3.1	Flow cytometry . . . . .	29
4.3.2	Confocal microscopy to qualitatively study cell internalization and gene expression . . . . .	32
<b>5</b>	<b>Conclusions</b>	<b>34</b>
<b>6</b>	<b>Future steps</b>	<b>35</b>
	<b>Bibliography</b>	<b>36</b>
<b>A</b>	<b>Supporting information</b>	<b>44</b>

# List of Tables

4.1	NTA mean size, PDI, concentration and mode of EVs, NPs, NP@EV 1:1, NP@EV 1:2 and NP@EV 1:10 are here reported . . . . .	23
4.2	Pearson's coefficient (PC) and Manders' coefficient (M1= fraction of green overlapping with red; M2= fraction of red overlapping with green) estimated for different images of NP@EV sample . . . . .	25
4.3	Fold change of BSA, CD63, CD81 and TGS101 in NP, NP@EV, EV and cell lysate samples. Values are normalized to the protein content in cell lysate . . . . .	28

# List of Figures

1	The encapsulation process is hereby summarized. THP-1-derived EVs were repeatedly frozen and thawed before being incubated with OM-pBAE NPs. The final characterization by DLS and the colocalization of polymer and lipid bilayer, along with the enhanced cellular uptake in vitro have confirmed the successful encapsulation.	iii
2.1	The possible biogenesis pathway for the formation of extracellular vesicles (EVs). Vesicles originated from multivesicular bodies or endosomes take the name of exosomes when secreted in the extracellular space. Microvesicles are generally bigger than exosomes and they form directly from the plasma membrane. When apoptotic events take place, apoptotic bodies, which are significantly bigger, are released.	8
4.1	Graphical representation of different encapsulation methods reported in literature	20
4.2	NTA means size, PDI, and mode of the NPs' control (CTRL), the NPs sonicated for 10 min (Sonic10') and 20 min (Sonic20'), and the NPs extruded 10 times (Ext10x) are here reported (a). NTA size distribution graphs of the NPs' control (CTRL), the NPs sonicated for 10 min (Sonic10') and 20 min (Sonic20'), and the NPs extruded 10 times (Ext10x) (b). Percentage of cells transfected (%GFP) by the non-treated NPs (NT), the NPs sonicated for 10 min (Sonic10') and 20 min (Sonic20'). Also, a negative control (CTRL-) of untransfected cells and a positive control (CTRL/) transfected by lipofectamine are included (c). NTA mean size, PDI, and mode of the EVs before freeze-thaw (CTRL) and after 0, 20, 40, 60, and 90 min are here reported (d). <i>Two-way analysis of variance (ANOVA) carried out between control and the samples, for the figure (a) and (d), and between every sample in Figure(c): *<math>p &lt; 0.05</math>, **<math>p &lt; 0.02</math>, ***<math>p &lt; 0.002</math>, ****<math>p &lt; 0.0001</math></i>	21

4.3	Graphical representation of the encapsulation method used in this work. EVs retrieved from the cell culture (1), disrupted EVs after the three <i>freeze-thaw</i> cycles (2), a mixture of cationic NPs and disrupted anionic EVs that will be attracted to each other by mean of the electrostatic interaction (3), encapsulated NPs into EVs after incubation time (4) . . . . .	22
4.4	(a)DLS hydrodynamic diameter distribution of EVs (green) and NPs (red). (b)DLS $\zeta$ -potential of EVs, NPs, NP@EV 1:2 and NP@EV 1:1. (c)NTA size distribution graphs of EVs, NPs, NP@EV 1:1, NP@EV 1:2, and NP@EV 1:10 . . . . .	24
4.5	Confocal microscopy of fluorescently labeled EVs and NPs are here reported both in the single fluorophore channels (Cy5 and NBD-PE) and the merged channel (Composite). Sample name is shown in the right hand side, scalebar = $10\mu m$ . . . . .	26
4.6	NP@EV 1:2 Cytoviva's hyperspectral image mapping. Channel name is shown in the top row of the figure . . . . .	27
4.7	Level of selected proteins analyzed by Western Blot . . . . .	29
4.8	Internalization assay performed with a flow cytometer using two different lasers to detect Cy5 and GFP/NBD-PE. Percentage of Cy5 (a) and GFP (b) detected in HEK293 at different time points for the negative control group (ctrl-), NP, EV, and different formulations of encapsulated NPs (NP@EV). Percentage of Cy5 (c) and NBD-PE (d) detected in THP1 at different time points for the negative control group (ctrl-), NP, EV, and NP@EV 1:2. On the x-axis are reported the negative control group (Ctrl-) along with the name of the treatments used in each group. <i>Two-way analysis of variance (ANOVA):</i> $*p<0.05$ , $**p<0.02$ , $***p<0.0001$ . . . . .	30
4.9	Immunofluorescence assay of THP-1 and imDC evaluated the expression of CD86 before and after differentiation protocol. Also, a negative control (CTRL-) without conjugated antibody was included. $***p<0.0001$ . . . . .	32
4.10	Confocal microscopy of EV, NP, and NP@EV after (a) 6h and (b) 48h of incubation. The sample name is reported on the left-hand side while the fluorophore shown in the channel is written in the top row. Scalebar = $20\mu m$ . . . . .	33
A.1	NTA size distribution graphs for EVs before (CTRL) <i>freeze-thaw</i> and after different recovering times (0, 20, 40, 60, 90 min) . . . . .	45

A.2	Confocal microscopy of fluorescent labeled EVs and NPs are here reported, including the controls we used to ascertain no cross-signaling was present. Channel name is reported above, while sample name is shown in the right hand side. scalebar = $10\mu m$ . . . . .	46
A.3	Excitation (dotted line) and emission (continuous line) graphs of fluorophores used to visualize through confocal microscopy the internalization of NPs and EVs into imDCs. . . . .	47



# Chapter 1

## Motivation and objective

### 1.1 Motivation

Immunotherapeutic strategies, applied to cancer diseases, function by relieving immunosuppression, thereby enabling immune-mediated tumor eradication. Various immunotherapy strategies have been developed to boost the immune response and among them, gene therapy-based immunotherapy shows great promise. Specific vaccines could be then designed in order to activate the patient's immune system against tumors, delivering antigen-encoding nucleic acids (NA) preventively in dendritic cells (DCs) in order to break tumor cells' immune tolerance. On this topic, the fundamental properties of gene carriers have been underlined over the years. The ideal gene carrier should protect the cargo from nonspecific interactions, immune detection, rapid clearance, and nucleases degradation at the same time as escaping the endosome for the successful delivery of NA [1, 2]. Between the possible carriers, oligopeptide-modified poly( $\beta$ -amino ester)s (OM-pBAEs) has been previously used to deliver different kind of NA such as plasmids, messenger RNA (mRNA) or small-interfering RNA (siRNA) into different kind of cells *in vitro* and *in vivo*. For this family of polymers changing the end-capping amino acid allows obtaining polyplexes with different physicochemical features like size or  $\zeta$ -potential, many of which have been vastly studied [3, 4, 5]. Furthermore, *Fornaguera et al.* [6] demonstrated the use of active targeting moieties can also retarget NPs to specific tissues *in vivo* thanks to the differential protein corona formed around NPs.

Besides the introduction of chemical modification on polymers' chain, extracellular vesicles (EVs) can be also exploited to improve gene delivery carriers such as polyplexes [7, 8, 9]. EV-based coatings enable the simultaneous targeting of multiple antigens and immunoevasive properties, while conventional nanoparticle functionalization aims to provide single features for the system. [10]. Evidence

shows the tendency for immune cell-derived EVs to be uptaken by the same cell type and their role in antigen presentation along with antigen-presenting cells (APC) from which the EVs are formed. These discoveries open the doors to new active targeting routes for the development of anti-cancer vaccination [11, 12].

## 1.2 Objective

In the previously described context, the goal of this work is to obtain extracellular vesicle-encapsulated pBAEs nanoparticles that become dendritic cells targeted gene carriers. More in detail, the objective can be divided as follow:

- i. Investigate different EV-encapsulation methods to find the most suitable for soft nanoparticles such as pBAEs NPs
- ii. Perform and characterize the encapsulation of pBAE NPs into EVs to establish a reproducible and robust methodology
- iii. Study the *in vitro* uptake of coated NPs and compare it with naked NPs

## Chapter 2

# Biological Background

### 2.1 Cancer therapies: from surgery to anticancer vaccines

Cancer is a leading cause of death, accounting for nearly 10 million deaths, or nearly one in six deaths, and an estimated 19.3 million new cases worldwide in 2020 [13]. More recent statics are compromised by the COVID-19 pandemic delay which affected both diagnostic and treatments of this tremendous healthcare burden, however, only in the United States are projected 1,958,310 new cancer cases and 609,820 cancer deaths by the end of 2023 [14]. Cancer is a complex disease where genetic alteration leads to abnormal cell behavior and uncontrolled proliferation. Moreover, neoplastic cells share a variety of hallmarks such as the acquired capabilities for sustaining proliferative signaling, evading growth suppressors, resisting cell death, enabling replicative immortality, inducing/accessing vasculature, activating invasion and metastasis, reprogramming cellular metabolism, and avoiding immune destruction. These hallmarks have been also reviewed and expanded recently, including emerging common characteristics of this disease. Such complexity supports the tremendous statistic reported above leading to the necessity to find successful treatments [15].

The “big three” of cancer treatments are undoubtedly surgery, chemotherapy, and radiotherapy, but there is no debate whether the best survival chance is given by early detection. Early detection of cancer involves two components: early diagnosis, which aims to identify symptomatic patients at the earliest stage possible, and screening, which involves testing asymptomatic individuals to detect cancer before any symptoms manifest. [16].

Between the possible treatments, **surgery** is the oldest one and the most effective single modality. However, advances in the surgery field are evident and almost

continuous over time. The newest technologies like minimally invasive and robot-assisted surgery minimize the effect on life quality and post-operation recovery. Surgery remains the primary treatment modality for most cancers, although surgical oncologists increasingly work as part of a complex multi-disciplinary team [17].

Another possible choice is represented by **chemotherapy**, especially for cancers complicated with metastasis. By different routes of administration, they are intended to reach systemic levels in order to inhibit uncontrolled proliferation of malignant cells, unfortunately suppressing also normal cells with high proliferation rates with clear side effects. Moreover, in a significant number of patients, the tumor does not respond to the therapeutic agents. Multi-drug resistance (MDR) can be developed by numerous mechanisms including decreased drug uptake, increased drug efflux, activation of detoxifying systems, activation of DNA repair mechanisms, or evasion of drug-induced apoptosis, thus the cell becomes resistant to a variety of structurally and mechanistically unrelated drugs in addition to the drug initially administered [18, 19].

**Radiotherapy** is a vital treatment method for cancer, utilized in the majority of cancer treatment plans in Western countries, particularly for localized tumors without complications. Cancer radiotherapy is limited by the maximum tolerated dose to adjacent normal tissues; thus, it can bring side effects as well as chemotherapy. Cancer stem cells are considered to be the primary source of radiation- and chemo-resistance, and tumor heterogeneity plays an important role in acquired radiation resistance, indicating that radiotherapy still needs to improve [20]. Alongside surgery, chemotherapy, and radiotherapy, **immunotherapy** has been established as complementary or alternative therapy thanks to the clinical successes of immune checkpoint therapy and DC-based immunotherapy. [17, 18, 20, 19, 21]. These new approaches find their groundwork in the insight that the immune system can effectively get rid of cancer cells during their initial transformation. This process is termed immunosurveillance. Although the immune system has the potential to individuate cancer cells, tumors are able to develop by the activation of the immunosuppression mechanism. In this context, the use of naturally derived or synthetically generated components to stimulate the immune system against tumor cells finds roots and represents a promising alternative. These therapies can either co-stimulate immune cells or block immune inhibitory pathways [1, 22]. Here some major immunotherapies groups developed over the years will be briefly introduced.

### *Oncolytic virus therapy*

Oncolytic viruses (OV) immunotherapy is an innovative approach to cancer treatment that utilizes natural or engineered viruses to selectively infect and destroy cancer cells. OVs are thought to promote anti-tumor responses through two primary mechanisms: direct reduction of tumor size by infecting and lysing tumor cells, and initiation of a systemic immune response against the tumor. [1].

### *Adoptive cell therapy*

Adoptive cell therapy (ACT) is a promising form of immunotherapy that exploits the antitumor properties of lymphocytes to eradicate primary and metastatic tumor cells. Lymphocytes are firstly isolated from the patient's peripheral blood, tumor-draining lymph nodes, or tumor tissue, expanded *ex vivo*, and reinfused back into the patient. Indeed, over the last two to three decades, autologous T-cell therapies have demonstrated their potential to induce dramatic clinical responses (and have become a viable therapeutic option) [1].

### *Immune checkpoint blockade*

Immune checkpoints are antibodies with the specific function of regulating the immune response in order to prevent autoimmunity and control the duration of the immune response. The ligand proteins are often overexpressed by tumor cells and do not allow the correct activation and response of immune cells against tumors. A promising approach has been the use of ant-immune checkpoint protein to block the immune-inhibitory pathways activated by cancer cells. This strategy, called "immune checkpoint blockade", has led also to FDA-approved therapy like Ipilimumab [23, 1, 22].

### *Cancer vaccines*

Conventional vaccines are generally prophylactic agents used to achieve long-term immunity against viruses, which are administered to healthy individuals in order to prevent the consequences of the disease after a possible exposition to the pathogen. However, vaccination strategies applied to the cancer field are not only prophylactic but also intended as a proper therapy. To date, only two cancer vaccines are prophylactic, and they are restricted to viruses-induced malignancies such as liver cancer caused by hepatitis B or genital cancer caused by the human papillomavirus. On the other hand, the main goal of therapeutic vaccines is to elicit strong antigen-specific CD8+ cytotoxic T lymphocytes (CTLs) mediated responses [24]. Therefore, as they are administered to eradicate the tumor, they will face the adverse tumor microenvironment (TME); in particular an immune-suppressed environment. Dendritic cells (DCs) are known to be the most effective antigen-presenting cells (APCs) and play a central role in coordinating innate and adaptive immune responses. Immature DCs possess high endocytic and phagocytic capacity permitting antigens capture, while later, upon recognizing a pathogen, DCs acquire a "mature" phenotype. At this stage, DCs are expressing a high level of major histocompatibility complex II (MHC-II) along with morphology changes and, most interestingly, the activation of the antigen-processing machinery. Mature DCs will consequentially move via the efferent lymphatic systems into the T-cell area of local lymph nodes, where they can induce the activation and differentiation of T-cells into effector cells, thereby initiating primary immune responses. Thus,

to overcome immune tolerance, cancer vaccines need to target a high quantity of antigens to dendritic cells (DCs) and subsequently activate and expand these cells with suitable agents [1, 25].

One of the main obstacles to the development of successful cancer vaccines is the identification of the most suitable antigens to use. The ideal antigen must be expressed only by tumor cells and not by normal cells, it must be present on all tumor cells in such a way that the cancer does not escape immune attack due to antigen downregulation and also, it must be highly immunogenic. Antigens can be administered to patients in different forms such as short-peptides, full-length proteins, recombinant viruses, and autologous or allogeneic tumor cells. Attempts based on those approaches have failed in different clinical phases, due to poor pharmacokinetics properties, inadequate immunogenicity, or, in the case of cell-based vaccines, to lack of tumor specificity. Knowing that APCs are extremely efficient at antigen presentation, DC-based vaccines were also developed. In this approach, tumor antigens are loaded *ex-vivo* in the patient's peripheral blood mononuclear cells (PBMC) derived DCs. After activation of the cells, they are reinfused back into the patient. Although these vaccinations have produced encouraging, albeit modest, results, such as the FDA-approved Sipuleucel-T for metastatic prostate cancer, the biotech-pharmaceutical industry did not adopt widely this method, due to the complexity of producing and administering the vaccine [24, 1, 22].

Besides more conventional antigen delivery methods, recent years have seen an increasing interest in developing nucleic acid (DNA and RNA) vaccines, since they meet the challenges of safety and efficacy. Nucleic acid (NA) vaccines also enable scalability, ease of production, consistency between batches, and safety. The initial failure of DNA vaccines was due to the adopted administration route. By needle injection, the DNA was deposited in intracellular space rather than inside. However, now it is well established that DNA, which is commonly a bacterial plasmid, must enter the cell nuclei in order to be transcribed into mRNA and express the correct polypeptide [26]. On the other side, mRNA only needs to be localized in the cytoplasm in order to be transcribed, facilitating the transfection. Moreover, RNA asserts safety advantages, being noninfectious and non-integrating. Normal cellular processes degrade it and its half-life *in vivo* can be modulated by various modification and delivery methods, which also can increase its efficacy [27]. However, direct RNA delivery has always been characterized by low immunogenicity *in vivo*, due to poor internalization and enzymatic degradation. In this context, gene carriers or vectors play a pivotal role, and they should exhibit fundamental properties such as protecting the cargo from nonspecific interactions, immune detection, rapid clearance, and nucleases at the same time as escaping the endosome for the successful delivery of cargo. Gene delivery carriers can be divided into two main categories: viral and non-viral vectors. Although viral vectors are predominant in clinical trials and are characterized by higher immunogenicity, new advances in

nanotechnology, material sciences, and NA chemistry has led to the emergence of non-viral gene delivery systems as promising strategy, overcoming the limitations of viral vectors [2].

## 2.2 OM-pBAEs nanoparticles for nucleic acid delivery

Among polymeric vectors, poly( $\beta$ -amino ester)s (pBAEs) have shown promising results, thanks to their spontaneous condensation with nucleic acids, forming discrete nanoparticles (NPs). pBAEs can be easily synthesized by Micheal's addition of primary amines to diacrylates. Further modification by end-capping oligopeptides on the acrylate-terminated polymer can provide specific functionality to the final nanoparticle. NPs obtained with oligopeptides-modified pBAEs (OM-pBAEs) condensed with different kinds of nucleic acid are easily cleaved by hydrolysis releasing the cargo, and therefore showed great transfection efficacy and biocompatibility, also of the metabolites of the polymer. The great transfection efficacy is also due to the positive surface charge which allows good interaction with the cell membrane and to the proton sponge effects, enhanced also by histidine end-capping, which allows the endosomal escape of the NPs after the internalization [28, 3, 4, 5]. pBAEs also showed intrinsic immunogenicity, as other polymers like poly(lactic-co-glycolic acid) (PLGA), polystyrene, and chitosan, being able to induce activation of immune cells, even without any costimulatory or inflammatory cues [29].

Despite these characteristics making pBAE a good candidate for NA delivery, this polymer is not exempt from limitations. The excessive positive charge has been also related to cytotoxicity, causing cell membrane disruption, and *in vivo* poor transport through tissue due to the electrostatic interaction with both cells and matrix protein and proteoglycans. Colloidal stability in physiological fluids can be also a conserving problem, causing aggregation of NPs and their consequent lowered transfection efficacy. One of the main problems in translating nanomedicine into clinical practices is the lack of targeting abilities of the nanoformulations. In this context, OM-pBAE NPs are affected by an uncontrolled and off-target release *in vivo*. There are several ways to obtain a more selective delivery of NA such as triggering the release by an external stimulus, the use of cleavable disulfide bonds, or the covalent grafting of specific active targeting moieties [28]. *Fornaguera et al.* [6] presented a proof of concept that demonstrates the possibility of introducing a targeting moiety to OM-pBAE NPs to retarget the biodistribution *in vivo*. In their work, the addition of retinol to the composition has been related to the formation of a different protein corona which caused a specific accumulation in the targeted organ, the liver. Another example is the mannose grafting to the backbone of pBAEs, in order to target the APCs which are characterized by an

overexpression of mannose receptors [30]. However, molecule grafting inevitably changes the flexibility of the polymer and will affect the NPs' formation. The stability and the condensation with NA must also be considered as the grafted moieties could interfere with the self-assembly and the electrostatic nature of this process. Moreover, this strategy is limited by the selectivity of the target, as more cell types may express the same receptors, and also by the fact that the targeting efficiency cannot be guaranteed for the impossibility to predict the exposure of the targeting molecule in the final NP conformation [28]. In this context, novel strategies have been investigated. The focus of this thesis has been on exploiting extracellular vesicles (EVs) to increase the specific uptake of the OM-pBAEs NPs into DCs [10, 12].

## 2.3 Extracellular vesicles: a natural targeting moiety

Micro-vesicles secreted by neoplastic cell lines were first noted in 1981 when the terms exosomes were first used [31]. Since then, studies of these particles have been going on and in the last years have received a lot of attention, leading to the formation of ISEV (International Society of Extracellular Vesicles), aimed to improve the research on EVs, also by publishing guidelines for researchers.

In the literature are reported different types of lipidic vesicles secreted by cells, that differ from each other by the subcellular origin. For example, vesicles generated by multivesicular bodies, or endosomes, take the name "exosomes". Other types can be the so-called micro-vesicles, or "ectosomes", generated directly from the plasma membrane, or, again, apoptotic bodies which are released during apoptotic events [32, 33, 34]. However, as for the nomenclature MI-SEV2018 [35] defines "extracellular vesicles" as a generic term

for lipidic bilayer particles without a functional nucleus, which, therefore, cannot

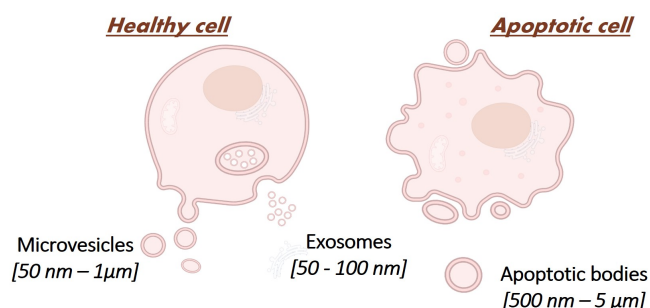


**Figure 2.1:** The possible biogenesis pathway for the formation of extracellular vesicles (EVs). Vesicles originated from multivesicular bodies or endosomes take the name of exosomes when secreted in the extracellular space. Microvesicles are generally bigger than exosomes and they form directly from the plasma membrane. When apoptotic events take place, apoptotic bodies, which are significantly bigger, are released.

replicate. They recommend the use of the term "EV" paired with other characterization references, such as size, density, or biochemical, rather than the subcellular origin, which needs specific markers in order to be verified.

EVs are involved in several intercellular communication mechanisms such as transporting proteins or peptides and delivering nucleic acids from the donor cell to the recipient cell. For example, EVs secreted by various cellular sources have several effects on the modulation of immune system activity, such as direct or indirect antigen presentation, antigen transfer, and maturation or activation of different immune cells [36]. While protecting the cargo from enzymatic degradation during the extracellular transporting, EVs are able to be internalized by the recipient cell by different routes. Phagocytosis, micropinocytosis, and cell surface membrane fusion have been reported as possible mechanisms by which EVs are taken up by recipient cells. However, endocytosis is considered to be the main mechanism by which the EVs enter endosomal compartments. This process has been found quite rapid, EVs can be identified inside the cell after just 15 minutes, and energy-dependent [37, 38]. Also, various proteins like tetraspanin, integrins, and immunoglobulins facilitated the endocytosis process and serve as natural targeting moieties [12]. EVs exhibit organotropic behavior in both local and long distant cell-to-cell communication. For example, immune cell-derived EVs have shown targeting ability to other immune cells, delivering unidirectionally microRNA from T cells to APCs [39]. However, controversial results have been collected. Multiple *in vivo* studies demonstrated non-specific accumulation in the liver and spleen, at levels comparable to liposomes vector or other nanoparticles administered systemically. In this context, choosing the appropriate parent cell type for the application it's crucial, but the natural targeting ability showed by some EVs make them good candidates for drug delivery carrier themselves or in combination with other nanomaterials [12].

The last decades showed an enormous interest in translating the EVs' natural vehicle ability into efficient drug delivery systems. One of the options is to use directly EVs loaded with active molecules or NA in order to deliver the cargo directly inside specific cell types. Many different parent cell-drug combinations have been tested for as many applications of interest. For example, *Haney et al.* [40] used catalase-loaded exosomes in order to treat Parkinson's disease. They detected great internalization in neurons in *in vitro* models and a significant neuroprotective effect in an *in vivo* model of Parkinson's disease. Another example is the use of exosomes to overcome MDR in cancer of common chemotherapeutic agents such as paclitaxel [41]. *in vitro* experiments on drug-resistant cells showed 50 times more cytotoxicity compared to naked paclitaxel and *in vivo* model murine lung carcinoma demonstrated a significant anticancer effect.

Another application of EVs in nanomedicine is to encapsulate NPs, as an improvement to the targeting ability of the delivery system. The main methods applied to NPs encapsulation are undoubtedly sonication and extrusion. Whether

it is forcing with pressure NPs and EVs through a porous membrane, or the use of ultrasound, these mechanical approaches force NPs to enter the EVs by contact and rearrange of the lipid bilayer around the NPs. These methods have been also applied in combination with electroporation or using saponins in order to permeabilize the cell membrane [10]. Another example, commonly considered less efficient, can be the freeze-thaw method, in which providing cycles of freezing at extremely low temperatures and thawing at room temperature (RT) allows the alteration and the temporary damage of EVs membrane and let the NPs to enter the vesicles prior to their reorganization in spherical structure [42]. Other works, instead, report exosome or lipid vesicle-coated NPs obtained through membrane fusion [43, 9, 7, 8]. This method requires NPs and EVs with opposite surface charges, thus the electrostatic interaction allows the membrane of EVs to engulf the NPs, forming the coating around the nanoparticles. To date, it is not clear which technique can be considered the foremost method of encapsulation, also because there is not a unique metric of evaluation. As a matter of fact, the correct encapsulation should be evaluated considering the nature of the NPs adopted.

In this thesis work, **we investigated the EVs encapsulation methods compatible with OM-pBAEs NPs, with the ultimate objective of retargeting the distribution aiming to DCs in order to produce an effective anticancer vaccine.** We investigated whether sonication, extrusion, freeze-thaw, or membrane fusion are suitable methods for this kind of NPs. Our results suggested that the application of freeze-thaw combined membrane fusion is a feasible method, by which we obtained EV-coated NPs with the same effectiveness in *in vitro* internalization but improved targeting moieties.

# Chapter 3

## Materials and methods

### 3.1 Materials

Bovine serum albumin (BSA), sodium acetate (AcONa), Loading Buffer, Tween-80, Gelatin (G2500; 9000-70-8; Lot SLBW1943), DAPI nucleus staining (D1306), and PBS were purchased from Sigma-Aldrich®, Cyanine 5 NHS ether dye was purchased from Lumiprobe. Fetal Bovine Serum (FBS), Dulbecco's Modified Eagle's Medium (DMEM), glutamine, penicillin, and streptomycin were obtained from Gibco®. RPMI-1640 medium was purchased by Biowest (L0501-500). Recombinant human interleukin 4 (rhIL-4), and recombinant human granulocyte-macrophage colony-stimulating factor (rhGM-CFS) were purchased from PeproTech®. Cell-Mask™ Orange Plasma membrane Stain was purchased from ThermoFisher Scientific. The cell lines used were human monocytic cells (THP-1; ATCC® TIB-202™), human spontaneously arising retinal pigment epithelia (ARPE-19, ATCC® CRL-2302™) and human embryonic kidney 293 cells (HEK293; ATCC® CRL-1573). NBD-PE was purchased from Avanti® Polar Lipids. Plasmid GFP (3486 bp) was produced and purified from *E.coli*.

Arginine and Histidine end-modified poly( $\beta$ )-amino ester (pBAE) the polymer was synthesized by the Group of Materials Engineering, following a two-step procedure described previously [3]. In brief, first, an acrylate-terminated polymer, C6 polymer, was synthesized in the Gemat group by addition reaction of primary amines with diacrylates (at 1:1.2 M ratio of amine:diacrylate). Finally, pBAE was obtained by end-capping modification of the resulting acrylate-terminated polymer with rather an arginine or histidine at each end.

## 3.2 Cell Culture

THP-1 cell lines were maintained in RPMI-1640 supplemented with 10% (v/v) fetal bovine serum (FBS), 100 units/mL penicillin G, 100  $\mu\text{g}/\text{mL}$  streptomycin, and 2 mmol/L L-glutamine. HEK-293 cell lines were maintained in DMEM supplemented with 10% (v/v) fetal bovine serum (FBS), 100 units/mL penicillin G, 100  $\mu\text{g}/\text{mL}$  streptomycin, and 2 mmol/L L-glutamine. All cells were cultured at 37 °C, under a 5% CO<sub>2</sub>/95% air atmosphere and passaged when arriving at 80-90% confluence.

### 3.2.1 Differentiation of THP-1 cell line

Briefly, THP-1 cells were cultured in a medium supplemented with 100 ng/mL rhIL-4 (recombinant human interleukin 4) and 100 ng/mL rhGM-CSF (recombinant human granulocyte-macrophage colony-stimulating factor) for 5 days to achieve differentiation. In order to verify the differentiation took place, a flow cytometer analysis was performed by staining the following surface markers: CD86.

## 3.3 Nanosystems preparation

### 3.3.1 Synthesis of OM-pBAE nanoparticles

The nanoparticles were prepared following the well-established protocol of the GEMAT group [44, 3]. Briefly, the mixture containing OM-pBAE and pPAX (a model plasmid, kindly donated by a collaborator of the group or pGFP (a plasmid DNA codifying for a green fluorescent protein) at ratio 25:1 was prepared by mixing equal volumes of pPAX 0.5 mg/mL and OM-pBAE 12.5 mg/mL in a solution of sodium acetate 12.5 mM at a pH of 5.2. The genetic material was added to the polymer solution, containing a mixture of 60% C6CR3-pBAE (R-pBAE) and 40% C6CH3-pBAE (H-pBAE), and mixed by vigorous pipetting, followed by 30 min of incubation at room temperature (V1).

After the incubation period, the mixture was nanoprecipitate in an equal volume (V1) of Milli-Q water. For all of the following experiments fresh nanoparticles (NPs) were used.

### 3.3.2 Labeling R-pBAE with fluorophore

In order to obtain fluorescence-detectable NP, the labeling of R-pBAE with Cyanine 5 NHS ester (Cy5) was performed as done previously in the GEMAT group [45]. Briefly, 35  $\mu\text{L}$  (1.6  $\mu\text{mol}$ ) of R-pBAE, 60  $\mu\text{L}$  (1.6  $\mu\text{mol}$ ) of Cy5 in DMSO (0.98  $\mu\text{mol}$ ), 4  $\mu\text{L}$  (29  $\mu\text{mol}$ ) of triethylamine (Et<sub>3</sub>N) and 270  $\mu\text{L}$  of DMSO were mixed. The solution was stirred in a water bath with a controlled temperature of 25°C

$\pm 2^{\circ}\text{C}$  for 20 h with a magnetic stir bar. The resulting product was precipitated in a mixture 7:3 v/v of diethyl ether:acetone. Then it was dried overnight and dissolved in DMSO to obtain a solution of 100mg/ml. The fluorescent-labeled polymer was used either at 0.2% v/v, for in vitro experiments, or 1% v/v, for colocalization analysis, of the total amount of R-pBAE needed to form NPs as previously explained.

### 3.3.3 Harvesting and purification of Extracellular Vesicles

The supernatant, freed of cells, was collected by mild centrifugation of culture medium, after 3 days of cell culturing, at 300xg for 5 minutes and stored at  $-80^{\circ}\text{C}$ . Once collected at an appropriate volume, the thawed supernatant was centrifugated at high-speed centrifugation, as described in our previous work [46] with Avanti®centrifuge j-26 XPI, using a JA-14.50 rotor (Beckman Coulter Life Science, USA) to collect extracellular vesicles (EVs). First, the supernatant was centrifugated at 10'000xg for 45 min at  $4^{\circ}\text{C}$  to eliminate cell debris. The recovered medium containing the EVs was then centrifugated a second time at 35'000xg for 70 min at  $4^{\circ}\text{C}$  and the pellet was resuspended in 1/50 of the initial volume of PBS. The samples were then stored at  $-80^{\circ}\text{C}$ . This method was followed to retrieve THP-1-derived EVs. The HEK-293-derived EVs were kindly donated by a Ph.D. student of the GEMAT group. These EVs were obtained from a genetically modified culture of the HEK-293 cell line in order to express a green fluorescent protein (GFP) on the double layer of the EVs.

### 3.3.4 Labeling of Extracellular Vesicles

The labeling of EVs was performed using NBD-PE, a phospholipid labeled on the head group with the NBD fluorophore, able to intercalate itself into the EVs' phospholipidic bilayer by passive incubation. A ratio of 5  $\mu\text{L}$  of NBD-PE (1mg/mL in PBS) each 100  $\mu\text{L}$  of EVs (at the concentration of approximately  $5 \times 10^{10}$  EV/mL) was mixed and incubated 1h at  $37^{\circ}\text{C}$  under agitation. Later, the solution was filtrated using a 50kDa cutoff Amicon®Ultra Centrifugal Filter Unit (Merck Millipore, USA) in order to eliminate the free label.

### 3.3.5 Sonication and extrusion methods

The extrusion was performed with Avanti®PolarLipid miniextruder using a 200 nm pore membrane for 10 times, while for the sonication, pBAEs NPs were put in a sonication bath, for 10 and 20 min. The analysis of the stability after the treatments was conducted in the NTA.

### 3.3.6 Encapsulation method

In this work, along with this electrostatic interaction, the encapsulation was performed by exploiting fast freezing cycles that enabled the disruption of EVs followed by a period of recovery of the same, along with incubation with the NPs. Briefly, a proper amount of EV solution was frozen at  $-80^{\circ}\text{C}$  in a mixture of acetone and dry ice and let thaw at room temperature. These cycles were repeated 3 times. After the last cycle, the NPs solution was rapidly added to EVs solution at different NP:EV ratios and gently pipetted to obtain a homogenous solution of both nanosystems and incubated for 1h at room temperature. This formulation will be referred to as NP@EV followed by an indication of the ratio (for example NP@EV 1:2, to indicate a ratio 1:2 of NP:EV). The ratio was calculated from the concentration of the samples of EVs and NPs, determined by Nanoparticles Tracking Analysis (NTA). The obtained formulation was always used freshly prepared for all the characterization and the following experiments.

## 3.4 Physicochemical characterization of the nanoformulations and *in vitro* studies

### 3.4.1 Dynamic Light Scattering (DLS) and Nanoparticles Tracking Analysis (NTA)

In dynamic light-scattering (DLS) instrument, the scattering intensity is recorded by a detector after an incident laser light encounters particles in suspension. The intensity fluctuations are elaborated through a digital autocorrelation function which is related to the diffusion behavior of particles and through the use of Einstein-Stokes equation to the hydrodynamic radius. As the scatter of light depends on the size of particles in suspension, larger aggregates even in a small amount will affect the measurements [47]. For this reason, EVs, but even more NP@EV, analysis with this technique can encounter some difficulties.

The nanoparticle tracking analysis (NTA) device combines laser light-scattering microscopy with a charge-coupled device (CCD) camera, which enables the visualization and recording of nanoparticles in solution. The NTA software is then able to identify and track individual nanoparticles moving under Brownian motion and relates the movement to a particle size according to a formula derived from the Stokes-Einstein [48].

In order to characterize the hydrodynamic size, polydispersity index (PDI), surface charge ( $\zeta$ -potential), size distribution, and sample concentration, analyses were conducted with both DLS and NTA. To determine the hydrodynamic size and PDI, a volume of  $50\ \mu\text{L}$  of NPs, prepared as previously described, or  $50\ \mu\text{L}$  of thawed EVs solution diluted 1:5 in PBS were put in a DLS micro-cuvette and analyzed

at 25 °C, 633 nm laser wavelength and 173° signal detector using a Zetasizer Nano ZS with the Zetasizer Software (Malvern Instruments, Worcestershire, UK). For the measurement of  $\zeta$ -potential, either NPs, EVs, or NP@EV samples were diluted 1:100 in Milli-Q water, in a final volume of 1mL, and samples were put in a Disposable Capillary cell (DTS1060, Malvern Instruments, Worcestershire, Inglaterra) and analyzed at the same condition as before by DLS. In order to determine size distribution and sample concentration, either NPs, EVs, or NP@EV samples were diluted 1:100 in PBS (or Milli-Q water for NPs), in a final volume of 1mL. The samples were run with the automated syringe pump in an NTA Nanosight NS300 (Malvern Panalytcs, United Kingdom). A PDI was also calculated as  $PDI = (\sigma/\mu)^2$ , where  $\sigma$  and  $\mu$  are NTA standard deviation and mean size respectively.

### 3.4.2 Hyperspectral microscopy

Samples were visualized, acquired using Exponent 7 software, and mapped from their hyperspectral images with a Cytoviva© high-resolution dark-field condenser (Auburn, AL, USA) which was coupled in an Olympus BX-43 optical microscope. Hyperspectral analysis imaging (HSI) was recorded using an ENVI 4.8 software in which the hyperspectral camera operated in the visible-near infrared range (VNIR) in the range of 400-1000 nm. A spectral library with a representative hyperspectral image was obtained from single components (EVs and NPs) separately by adding 10  $\mu$ L to a microscope glass slide. The NP@EV sample, freshly prepared, was placed on a microscope slide (10  $\mu$ L) with a coverslip and observed. Hyperspectral images of NP@EV were obtained and spectral similarities that matched with the spectral library of EVs and NPs facilitated the mapping process.

### 3.4.3 Western Blot

The concentration of proteins in the analyzed samples was assessed using the Pierce™ BCA Protein Assay kit (Thermo Fisher Scientific, Waltham, MA, USA; 23225) according to the manufacturer's instructions. A western blot was performed to evaluate EVs protein content. Briefly, isolated EVs were lysed in reducing sample buffer [0.25 M Tris-HCl (pH 6.8), 40% glycerol, 8% SDS, 5% 2-mercaptoethanol and 0.04% bromophenol blue] or non-reducing sample buffer (without 2-mercaptoethanol) and boiled for 10 minutes at 65°C. Proteins were resolved by SDS-PAGE (SDS-polyacrylamide gel electrophoresis) 10% or 15% (for TGS101 and CD63 or BSA and CD81, respectively), transferred to polyvinylidene fluoride membranes, blocked in 5% non-fat powdered milk in PBS-T (0.5% Tween-20) and probed with antibodies. Antibodies applied with reduced samples were purified anti-TSG101 antibody (Cat. 934301, Biolegend) and Bovine Serum

Albumin Polyclonal Antibody (BSA; Cat. A11133, Invitrogen). CD81 Antibody (1.3.3.22; sc-7637, Santa Cruz Biotechnology) and CD63 Antibody (MX-49.129.5; sc-5275, Santa Cruz Biotechnology) were applied to non-reduced samples. For detection, goat pAB to MS IgG (HRP; Mouse; GR3219929, Abcam), HRP Goat Anti-rat igG (minimal x-reactivity; Cat 405405, Biolegend), goat anti-Rabbit, Rat IgG (H+L) secondary (NB7160, Novus Biologicals) and Pierce® ECL Western Blotting–substrate (Thermo Fischer Scientific, Rockford, IL, USA) were used, while the membrane was analyzed with an Amersham™ImageQuant™800 biomolecular imager (Cytiva Life Sciences, USA).

### 3.4.4 Flow cytometry

The analysis of the CD86, a marker of DCs differentiation, was performed in order to verify the correct differentiation of the THP-1 cell line into imDCs. Briefly, an amount of  $5 \times 10^5$  of cells/sample was retrieved from each cell culture, fixed in formalin 10% for 20 min at 4 °C, and then washed in PBS. The samples were resuspended in a blocking buffer containing 1% (v/v) BSA in PBS, for 20 min at 4°C. After another washing step in PBS, the samples were incubated for 1h at RT with the primary antibody anti-human CD86 conjugated with PE fluorophore (BioLegend, San Diego, USA), following the manufacturer’s instructions. The unbound antibodies were then washed in PBS and the samples were analyzed with Flow cytometer ACEA (NovoCyte, Santa Clara, USA).

In order to assess the ability of the system to enter the cell, in vitro analyses were conducted using 0.2% Cy5 labeled NPs and labeled EVs (either with NBD-PE or GFP) thus the uptake could be measured. The flow cytometer analysis was conducted on two different cell lines: the THP-1 cell line and the HEK-293 cell line. For each cell line, EVs retrieved from each own cell culture were used.

Briefly, cells were seeded on a 96-well plate at a concentration of  $2 \times 10^4$  cells/well. Seeded cells were incubated at 37°C in a 5% CO2 atmosphere for different times (24h, 36h, 48h for THP-1 cell lines and 4h, 24h, 48h for HEK-293 cell line) with the corresponding treatments. The amount of treatment was calculated to obtain a final concentration of 0.3  $\mu\text{g}$ /well of nucleic acid. After the incubation timings were reached, the cells were washed with PBS and fixed in formalin 10%. Since the cell lines used were cultured in suspension every washing step was done with a previous centrifugation step at  $310 \times g$  for 5 min in order to sediment the cells at the bottom of the plate. The samples were then analyzed with Flow cytometer ACEA (NovoCyte, Santa Clara, USA).

### 3.4.5 In vitro transfection study

For 96-well plates, the procedure of transfection was the following. ARPE-19 cells were seeded on the plate at a concentration of  $2 * 10^5$  cells/well. Seeded cells were incubated at 37°C in a 5% CO<sub>2</sub> atmosphere for 48h with the non-treated, sonicated (10 min and 20 min) nanoparticles. pBAE/nucleic diluted in culture medium at a final concentration of 1,8 µg/well of nucleic acid. After the transfection timings were reached, the cells were washed with PBS and fixed with formalin 10% ready to be analyzed with the flow cytometer.

### 3.4.6 Confocal microscopy

In order to verify the colocalization of NP and EV after the encapsulation protocol, a confocal image was taken. Briefly, the EV stained with NBD-PE and the NP labeled with 1% Cy5 were used as previously described to form NP@EV. An amount of 10 µL of the sample was deposited onto the glass and covered with the coverslip, sealed eventually with nail polish, and analyzed with a confocal microscope Leica DMi8 S.

To visualize and confirm with another method the ability of the encapsulated system to enter the cell, the same labeling as the previous protocol was used. Cells were seeded in a 24-well plate containing a cover glass with 500 µl of gelatin 0.1%, the gelatin was incubated for 30 min, and the excess was removed by aspiration. imDCs were seeded at a concentration of  $3 * 10^4$  cell/well and incubated for 24h at 37°C. After short (6h) and large (48h) incubation timings with the treatments (with the same condition as in the previous protocol). The cells were fixed in formalin 10% for 20min and permeabilized with PBS-Tween80 0.1%, washing the coverslip with PBS in each step. Additional, staining for cell nucleus (DAPI, 1:10'000 in PBS for 10 min at RT) and membrane (CellMask™ Orange, 1:1'000 in PBS for 10 min at RT) was used, once again washing the coverslip with PBS in each step.

The cover glass was placed onto the glass microscope slide and then the cellular uptake of the nanoparticles was observed by using a confocal microscope Leica DMi8 S.

In order to visualize correctly the uptake, cells' nuclei were stained with DAPI while the membrane was stained with CellMask®Orange. All of the excitation/emission (Em/Ex) wavelengths are reported in figure A.3, along with Fluorescent SpectraViewer's graphs (Thermo Fisher Scientific).

## 3.5 Statistical analysis

Statistical analysis was performed by one/two-way ANOVA analysis with GraphPad Prism 8.0.1.

All images obtained from confocal microscopy analysis were elaborated with the software Fiji /ImageJ 1.52v (Wayne Rasband, National Institutes of Health, USA).

Graphical representations of various methodologies or experimental protocols reported throughout this thesis were created with [biorender.com](https://biorender.com).

# Chapter 4

## Results and discussion

### 4.1 Methodology of encapsulation set up

The literature presents a variety of different approaches [49, 10] in order to encapsulate either chemical compounds, molecules, macromolecules, or nanoparticles of different sizes into the EVs.

**Incubation** method is used to load EVs by incubating the latter with a cargo of interest, especially hydrophobic interfaces. To expand the packing efficiency, **sonication** and **extrusion** strategies have been also established. Sonication and extrusion are techniques acquired from the liposomal species, which can cause the transformation or twisting of EVs' membrane to access the introduction of cargo. These methods will be further discussed in this chapter. **Saponin assisted treatment** of permeabilization can provide an even higher level of internalization, being an active compound that can form complexes with cholesterol on the surface of EVs and create holes, therefore enhancing membrane permeability [50]. In contrast to cellular membranes, EVs exhibit a more rigid lipid bilayer due to aggregation of sphingomyelin, cholesterol, and ganglioside. Thus, it can be more difficult to insert hydrophobic substances from cells to vesicles [42]. The **freeze-thaw** method allows EVs' drug-loading with a straightforward technique. EVs are mixed with drugs, and then they undergo a few cycles of freezing at -80 °C in liquid nitrogen and thawing at RT [49].

For what concern EVs loaded with nanoparticles, to date, a majority of the nanoparticles have been metallic in nature including gold nanoparticles, iron oxide nanoparticles, (IONS), and gold-IONS (GIONS). However, there have been a few examples of poly(lactic-co-glycolic acid) (PLGA) nanoparticles and metal-organic framework (MOF) nanoparticles coated with EVs [10]. For example, *Illes et al.*[43] reported for the first time an exosome-coated MOF NPs as a smart and efficient drug delivery system with “onboard-trigger”. MOF NPs were successfully coated with

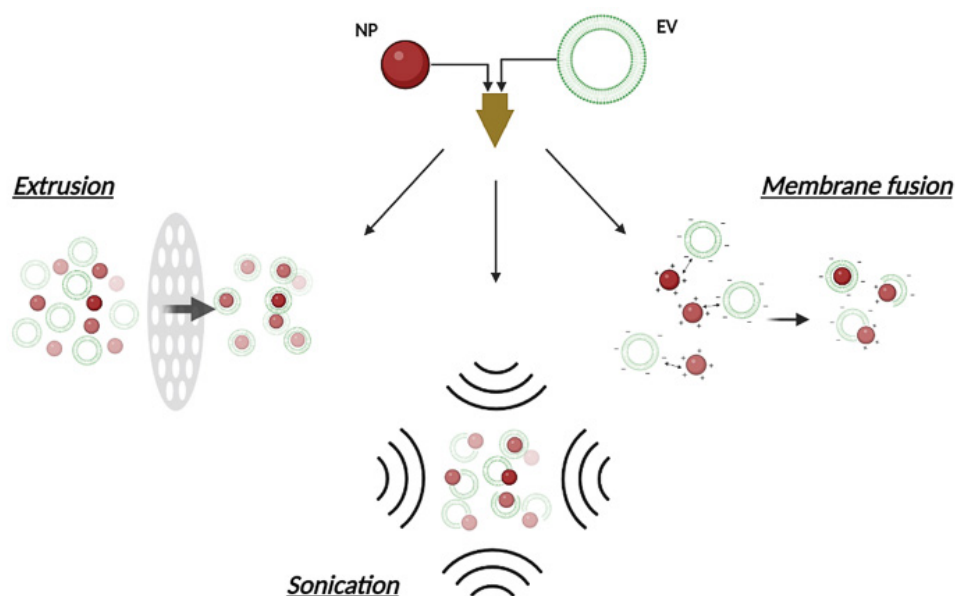


**Figure 4.1:** Graphical representation of different encapsulation methods reported in literature

exosomes derived from HeLa cell culture by means of the membrane fusion method. Examples of PLGA nanoparticles coated with EVs or cell-membrane-derived vesicles exploited sonication and extrusion methods, which are found to be the most common encapsulation methods (figure 4.1) [51, 52, 10].

### *Sonication and extrusion methods*

Both extrusion and sonication methods require that NPs, previously incubated with EVs, should undergo these processes without compromising their morphology or functionality. Therefore, we evaluated preliminary the capability of pBAEs NPs to survive these treatments, before trying to perform the encapsulation into the EVs. Size (mean and mode values) and PDI are reported in figure 4.2a, while size distribution is reported in Figure4.2b. The 10 min sonication (Sonic 10') slightly increased the mean size of the NPs, from around 130 nm to 154 nm, while PDI and size (mode value) remains unvaried. At 20 min sonication (Sonic 20') we can observe a considerable increase in mean size, mode, and PDI underlining a partial degradation of the NPs' morphology. On the other hand, NPs are shown not capable of surviving the extrusion, as can be seen from the high PDI (around 0.500), the mode of 33 nm, and even more clearly by the size distribution graphs. Thus, we continued only with sonicated NPs.

To evaluate the functionality of sonicated NPs, an in vitro transfection assay was also performed on ARPE-19 cell line, which represents a suitable transfection host. As shown in Figure4.2c, 10' of sonication did not affect the transfection

efficiency compared to the non-treated (NT) sample, while 20' of sonication slightly decrease the percentage of transfected cells.

In conclusion of these preliminary experiments, the extrusion method has been discarded. Despite the fact the pBAEs NPs could undergo a sonication process without losing their transfection ability, encapsulation with sonication methods was not carried out in this work but represent a suitable alternative or a possible improvement to the actual strategy adopted here. Thus, neither of them was used due to their aggressiveness to soft nanoparticles.

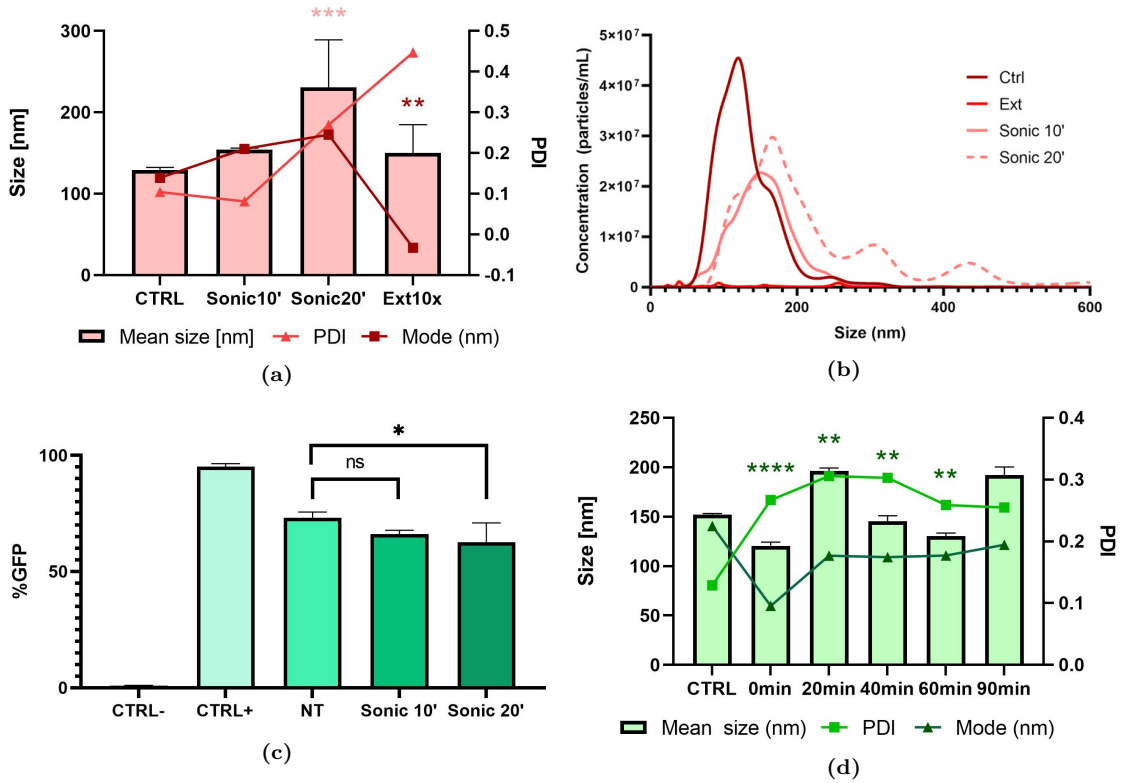


**Figure 4.2:** NTA means size, PDI, and mode of the NPs' control (CTRL), the NPs sonicated for 10 min (Sonic10') and 20 min (Sonic20'), and the NPs extruded 10 times (Ext10x) are here reported (a). NTA size distribution graphs of the NPs' control (CTRL), the NPs sonicated for 10 min (Sonic10') and 20 min (Sonic20'), and the NPs extruded 10 times (Ext10x) (b). Percentage of cells transfected (%GFP) by the non-treated NPs (NT), the NPs sonicated for 10 min (Sonic10') and 20 min (Sonic20'). Also, a negative control (CTRL-) of untransfected cells and a positive control (CTRL/) transfected by lipofectamine are included (c). NTA mean size, PDI, and mode of the EVs before freeze-thaw (CTRL) and after 0, 20, 40, 60, and 90 min are here reported (d). Two-way analysis of variance (ANOVA) carried out between control and the samples, for the figure (a) and (d), and between every sample in Figure(c): \* $p < 0.05$ , \*\* $p < 0.02$ , \*\*\* $p < 0.002$ , \*\*\*\* $p < 0.0001$

### Freeze-thaw and membrane fusion methods

The advantages of employing freeze-thaw methods include their simplicity, a moderate loading capacity (regarding encapsulation of compounds such as active molecules, proteins, or genetic material), and membrane fusion [49]. Mac Donald et al.[53] reported in 1983 how freeze-thaw cycles promote lipid mixing in the liposomal membrane, suggesting that conformational changes, breakdown, and rearrangement of lipidic vesicles occur during repeated fast freezing and thawing processes.

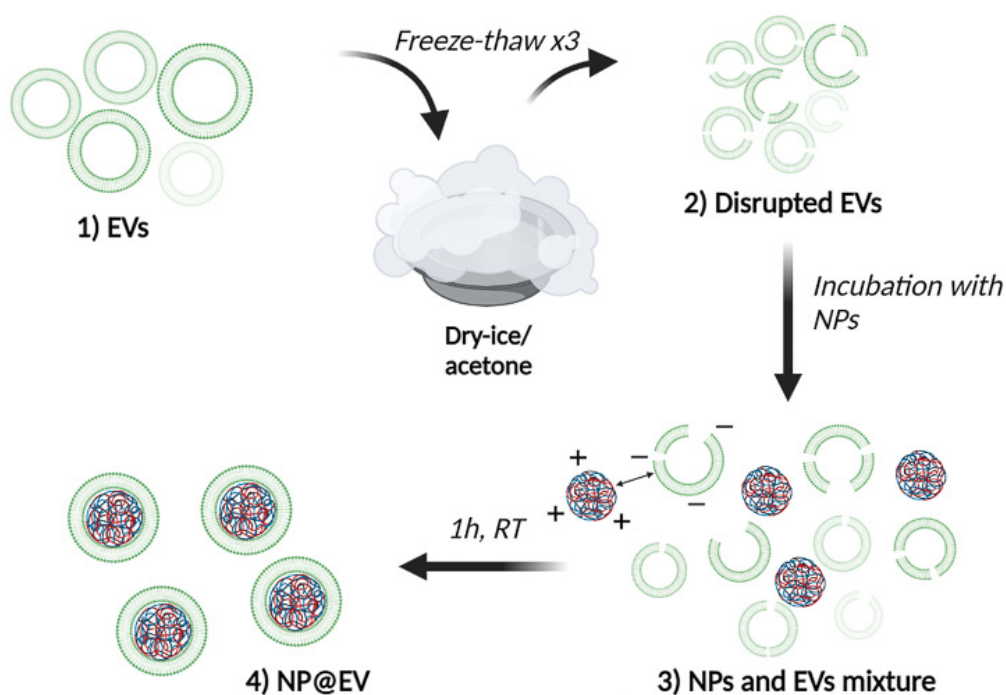


**Figure 4.3:** Graphical representation of the encapsulation method used in this work. EVs retrieved from the cell culture (1), disrupted EVs after the three *freeze-thaw* cycles (2), a mixture of cationic NPs and disrupted anionic EVs that will be attracted to each other by mean of the electrostatic interaction (3), encapsulated NPs into EVs after incubation time (4)

In our work, we also evaluated preliminary the **effects of freeze-thaw cycles** on EVs. After three cycles of freeze-thaw, in a mixture of dry-ice and acetone ( $-80^{\circ}\text{C}$ ) and at RT for a couple of minutes (just the time needed to have the sample thawed) respectively, the samples were analyzed with NTA after different recovery times (carried out at RT): 0, 20, 40, 60, 90 minutes. Concerning figure 4.2d, right after freeze-thaw cycles both mean size and mode decrease, underlying that fast freezing process breaks down EVs, which rapidly reassemble themselves into smaller vesicles. Moreover, PDI increases rapidly after the freeze-thaw cycles and tend to lower themselves over the 90 min, suggesting a partial recovery of the initial

structure, indicated also by the increasing mode and mean size, recuperating initial values. Besides, aggregation on EVs can be noted in the size distribution graphs (figure A.1).

Along with encapsulation methods based on freeze-thaw, also electrostatic interaction has been exploited in order to cloak negatively charged lipid vesicles over cationic nanoparticles. As previously reported [9, 7, 43], negatively charged liposomes can entrap cationic nanoparticles of various nature (polyplexes or Mesoporous Silica Nanoparticles) by spontaneous charge interaction, also called membrane fusion. *Akita et al.*[8] developed multi-layered nanoparticles exploiting the capability of negatively charged small unilamellar vesicles (SUVs) to surround the cationic polyplexes and, triggered by the electrostatic interaction, fuse themselves to form a lipidic double layer coating.

In our work, since none of the methods can be applied to pBAE NPs, we decided to apply first the freeze-thaw cycles to EVs, in order to provide disrupted and smaller vesicles, and then we incubated them with cationic pBAE NPs to exploit the spontaneous electrostatic interaction for the final encapsulation (figure 4.3).

## 4.2 Characterization of the nanoformulations

### 4.2.1 Physico-chemical characterization: size, surface charge, polydispersity and concentration

Preliminary investigation showed in the previous section underlined soft nanoparticles such as pBAEs NPs could be compromised during harsh conditions processes like extrusion or sonication. On the other hand, freeze-thaw can induce conformational changes in the lipidic bilayer of EVs facilitating the interaction with positively charged NPs to form a coating around them. For these reasons, our deeper investigation focused on the EV-encapsulated NPs obtained through incubation of pBAEs NPs with previously freeze-thawed EVs (the detailed method is reported in Chapter 3, "Material and methods").

**Table 4.1:** NTA mean size, PDI, concentration and mode of EVs, NPs, NP@EV 1:1, NP@EV 1:2 and NP@EV 1:10 are here reported

	Mean Size [nm]	PDI	Concentration [particles/mL]	Mode [nm]
<i>EVs</i>	126,1	0,144	8,26E+08	100,7
<i>NPs</i>	141,9	0,083	3,28E+09	120,3
<i>NP@EV 1:1</i>	207,3	0,229	6,99E+08	204,4
<i>NP@EV 1:2</i>	219,8	0,149	7,66E+08	170,0
<i>NP@EV 1:10</i>	119,5	0,285	2,01E+08	97,0

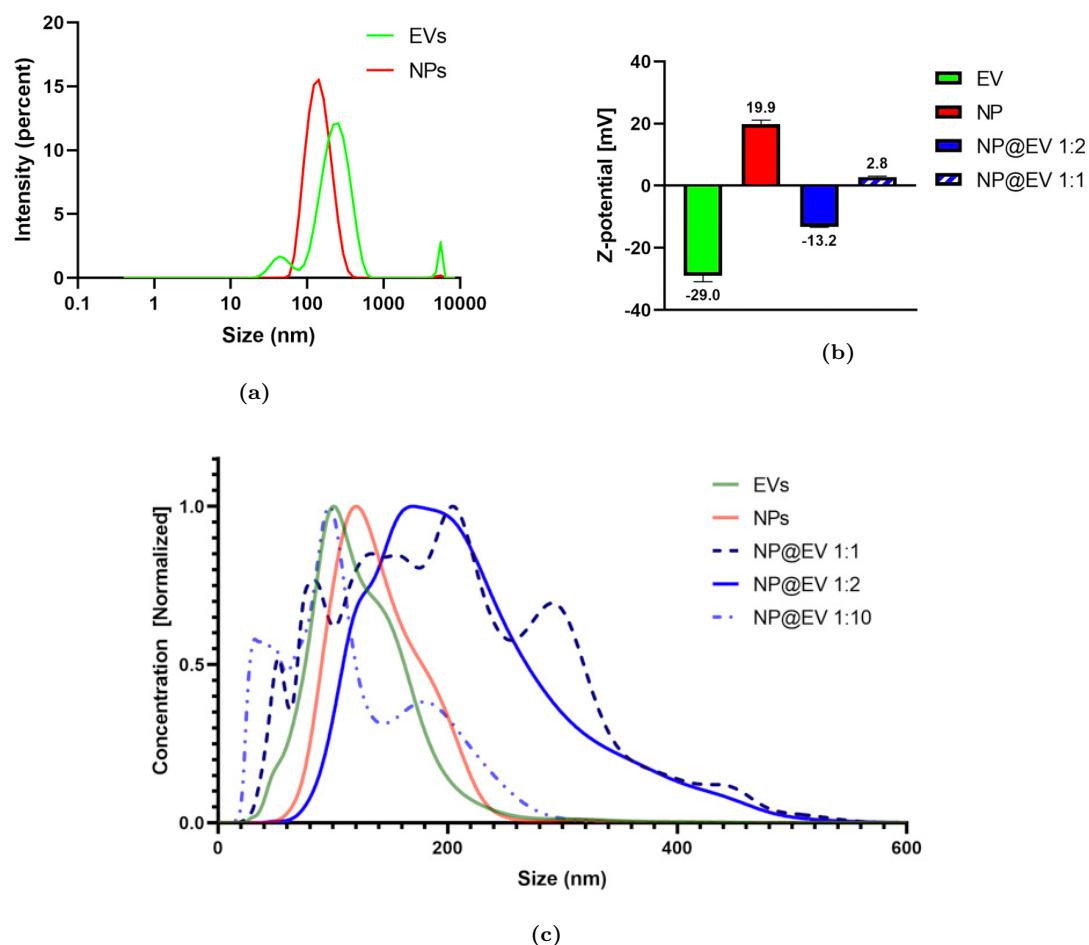


**Figure 4.4:** (a)DLS hydrodynamic diameter distribution of EVs (green) and NPs (red). (b)DLS  $\zeta$ -potential of EVs, NPs, NP@EV 1:2 and NP@EV 1:1. (c)NTA size distribution graphs of EVs, NPs, NP@EV 1:1, NP@EV 1:2, and NP@EV 1:10

DLS analyses of hydrodynamic diameter and  $\zeta$ -potential are shown in Figure 4.4a and 4.4b. Monodispersed NPs have a PDI of around 0.140, while pristine EVs show three different peaks and a PDI of around 0.330. EV samples have two major populations of 50 nm and 250 nm, while NPs have a hydrodynamic diameter of around 130 nm. To overcome the limitation of DLS in detecting particles' larger aggregates, NTA was conducted on NPs, EVs, and three different formulations of NP@EV (1:1, 1:2, 1:10 v/v ratio of NP:EV). As reported in the normalized NTA size distribution (figure 4.4c) and the table 4.1, between the three different formulations only the 1:2 ratio results in a monodisperse system (PDI=0.149) with an increased mean size and mode respect EVs and NPs alone. The bigger aggregates in the 1:1 ratio could be justified by the excess of NPs, which cannot

be fully coated and may have the tendency to aggregate with other EVs, driven by electrostatic forces. On the other side, in the 1:10 ratio the mode around 100 nm, as the EVs alone, suggests that the majority of EVs did not interact with NPs.  $\zeta$ -potential analysis (figure 4.4b) of EVs and NPs alone report a surface net charge of  $-29mV$  and  $19.9mV$  respectively, while different values are reported in the case of NP@EV, depending on the ratio. Here, the slight positivity of NP@EV 1:1 seems to agree with the idea that not all of the nanoparticles have been fully coated, a situation caused by the lack of EVs. These preliminary results regarding size, polydispersity, and  $\zeta$ -potential of the encapsulated NPs showed the best ratio in order to obtain monodispersed small enough NP@EV, with lower surface net charge respect EVs alone, is the formulation using a ratio NP:EV of 1:2, which have been used for further studies, presented in the next sections.

The fact that its surface charge is negative could be an indication of the EVs bilayer surrounding the NPs, although, for the moment, the exact insight structure of the complexes cannot be defined with the techniques used here.

## 4.2.2 Determining the NP@EV complexation by fluorescent microscopy

In order to confirm the interaction between NPs and EVs, a confocal image of the NP@EV 1:2 sample was taken after labeling the two nanosystems with two different fluorophores, as previously explained in the experimental section.

in Figure4.5 the channel of Cy5 (red) and NBD-PE (green) are reported, representing the NPs and the EVs respectively, and the merged image of the two channels. The yellow signals, shown in the merged images, are the result of the colocalization of NPs with the EVs, confirming the hypothesis of an interaction between the two systems, although the morphology of the complexes cannot be clarified yet. The Supporting

Information also reported the controls used to verify the correct attribution of the signals to either NPs or EVs, those controls were EVs alone (labeled) and the NP@EV where only NPs were labeled in order to verify eventual cross-signaling between the two systems, while no image of NPs alone was taken. To be noted, all the samples were analyzed at the same concentration and using the same fluorescent label, although some samples showed

**Table 4.2:** Pearson’s coefficient (PC) and Manders’ coefficient (M1= fraction of green overlapping with red; M2= fraction of red overlapping with green) estimated for different images of NP@EV sample

	PC	M1	M2
#1	0,525	0,444	0,426
#2	0,479	0,343	0,362
#3	0,529	0,395	0,49
#4	0,541	0,526	0,444
#5	0,536	0,417	0,516
#6	0,557	0,475	0,492
#7	0,388	0,416	0,199
Mean	0,508	0,431	0,418

lower intensity and lower particle concentration in the image (figure A.2), due to technical difficulties in managing liquid sample on the microscope glass.

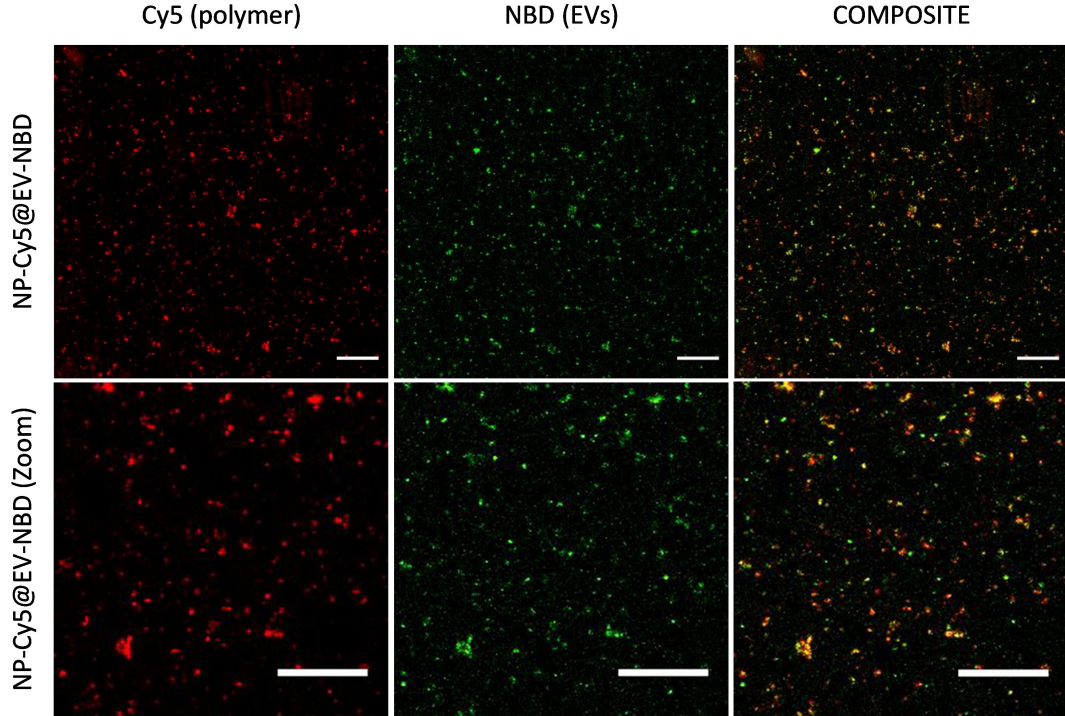


**Figure 4.5:** Confocal microscopy of fluorescently labeled EVs and NPs are here reported both in the single fluorophore channels (Cy5 and NBD-PE) and the merged channel (Composite). Sample name is shown in the right hand side, scalebar =  $10\mu\text{m}$

A further analysis was performed on the NP-Cy5@EV-NBD sample's image with the help of JACoP (Just Another Colocalization Plug/in, [54]). The colocalization of the two fluorophores was estimated through Pearson's coefficient and Manders' coefficient. Pearson's coefficient (PC) value can range from 1 to -1, with 1 standing for complete positive correlation and -1 for a negative correlation, with zero standing for no correlation. Manders' coefficient (MC) derives from PC and this new coefficient will vary from 0 to 1, the former corresponding to non-overlapping images and the latter reflecting 100% colocalization between both images. The MC is very sensitive to noise. To circumvent this limit, coefficients may be calculated setting the threshold to the estimated value of background instead of zero. The results reported in Table 4.2 are the estimation of seven different images from the confocal microscope of Pearson's coefficient (PC) and Manders' coefficients (M1, a fraction of green overlapping with red; M2, a fraction of red overlapping with green). MC was calculated using a different threshold in order to exclude the background noise. For both coefficient higher values indicates a better colocalization of the

two fluorophores, meaning in some areas of the analyzed sample more NPs could be in close contact with the EVs. Both coefficients report an average estimation between 40 and 50% of colocalization, indicating a good colocalization of EVs and NPs, although not all the nanoparticles seem fully coated.

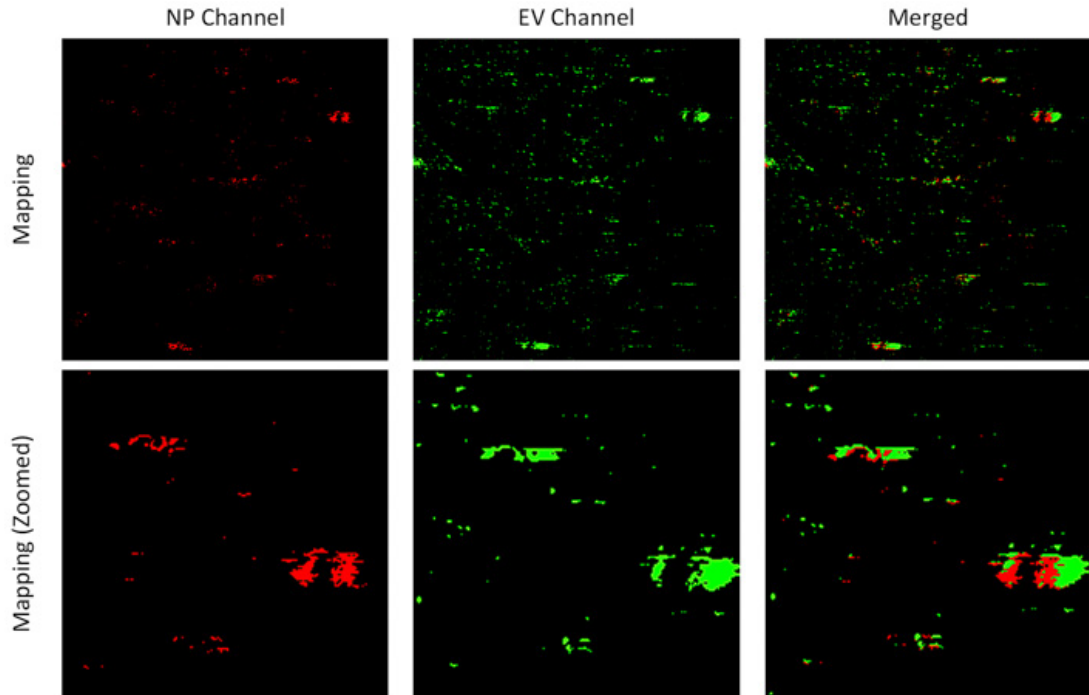


**Figure 4.6:** NP@EV 1:2 Cytoviva's hyperspectral image mapping. Channel name is shown in the top row of the figure

To verify the information about the coating of the NPs with EVs with another technique, an analysis with a hyperspectral microscope was performed. Dark field microscopy anchored with hyperspectral imagery (HSI) is a novel optical approach that allows the identification of specific components in the biological environment, dark field hyperspectral (HSI) microscopy provides a high contrast optical image, suitable for the observation of low-contrast objects, usually not visible by conventional bright field microscopy, while HSI yields a hyperdata cube with continuous spectral and spatial information in one measurement. Nanocomposites, at the single particle level or collectively, can be then tracked by exploiting the dark field optics and characterized by their spectral signatures.

In the figure 4.6, it is reported the mapping performed on the NP@EV 1:2 sample after creating the two separate libraries referring to the nanoparticles and the extracellular vesicles. It is clear how the image appears similar to the confocal

image, as before we have the copresence of the two-material combined together, even though the morphology seems far from the original nanoparticle or EV. Thus, it is clear to confirm that the complexes between NPs and EVs are formed.

### 4.2.3 Western Blot analysis to confirm nanostructures are EVs

The minimal information for studies of extracellular vesicles revisited in 2018 (MISEV2018, [35]), established common guidelines for researchers in order to correctly and uniformly present the results of studies on EVs. It established at least 3 categories of protein that should be evaluated in sample material:

- i. To demonstrate the presence of a lipid bilayer in the material analyzed, at least one transmembrane or glycosylphosphatidylinositol (GPI)-anchored extracellular protein must be shown. In this case, we analyzed the presence of TGS101.
- ii. To demonstrate that the material analyzed contains more than open cell lysate, at least one cytosolic/periplasmic protein with lipid or membrane protein-binding ability must be shown.  
The presence of two different tetraspanins (CD63, CD81) were evaluated.
- iii. Purity controls include proteins found in most common co-isolated contaminants of EV preparations: depending on the source of EVs. In this case, we evaluated the presence of Bovine Serum Albumin (BSA) in the EVs sample.

**Table 4.3:** Fold change of BSA, CD63, CD81 and TGS101 in NP, NP@EV, EV and cell lysate samples. Values are normalized to the protein content in cell lysate

	BSA	CD63	CD81	TGS101
<i>NP</i>	0,00	0,01	0,02	0,12
<i>NP@EV</i>	0,01	0,90	2,59	0,10
<i>EV</i>	0,04	0,97	4,91	0,59
<i>Cell</i>	1,00	1,00	1,00	1,00

A western blot analysis was conducted in order to verify the presence of these markers (1-3) in THP-1 cell lysate, THP-1 derived EVs, NP@EV and a sample containing only NPs (figure 4.7). In table 4.3 are reported the quantification of protein content normalized to the cell lysate. For what concern the BSA contaminants, their presence is significantly lower in the EV sample compared to the cell lysate, as well as the other sample. The protein markers CD63 and

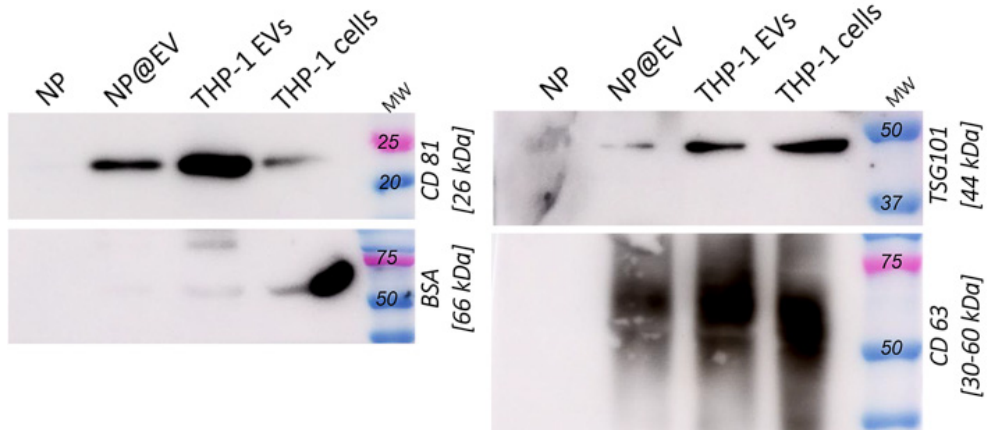


**Figure 4.7:** Level of selected proteins analyzed by Western Blot

TGS101 content decrease in the EVs sample and after the encapsulation process. An exception is represented by the CD81 marker which appears to be overexpressed in the EV sample, compared to the cell lysate, but the quantification shows a reduction after the encapsulation process. In fact, in the literature it is reported that freeze-thaw cycles could degrade or rearrange protein markers expressed on the EVs' surface [49], which is consistent with a reduction in protein content for all of the markers here analyzed.

### 4.3 *In vitro* uptake studies

#### 4.3.1 Flow cytometry

To evaluate the capability of our system to be internalized by cells we performed a flow cytometry assay after treating HEK-293 or THP-1 cell line with EVs and NPs labeled with GFP/NBD-PE and Cy5 respectively.

Firstly, we compared the ability of naked NPs, EVs, and two different formulations. The two formulations were:

- NP@EV 1:2, which is the most promising formulation from previous experiments.
- NP@EV 2:1, a formulation with an inverted ratio, made to verify if a lower amount of EVs still could enter the cell after the encapsulation process with an excess of NPs.

We assessed the ability of EV-coated NPs to be internalized using an *in vitro* model

by HEK-293 cell line, a permissive cell line (figure 4.8a,4.8b). In this experiment, only HEK-293 derived EVs were used.

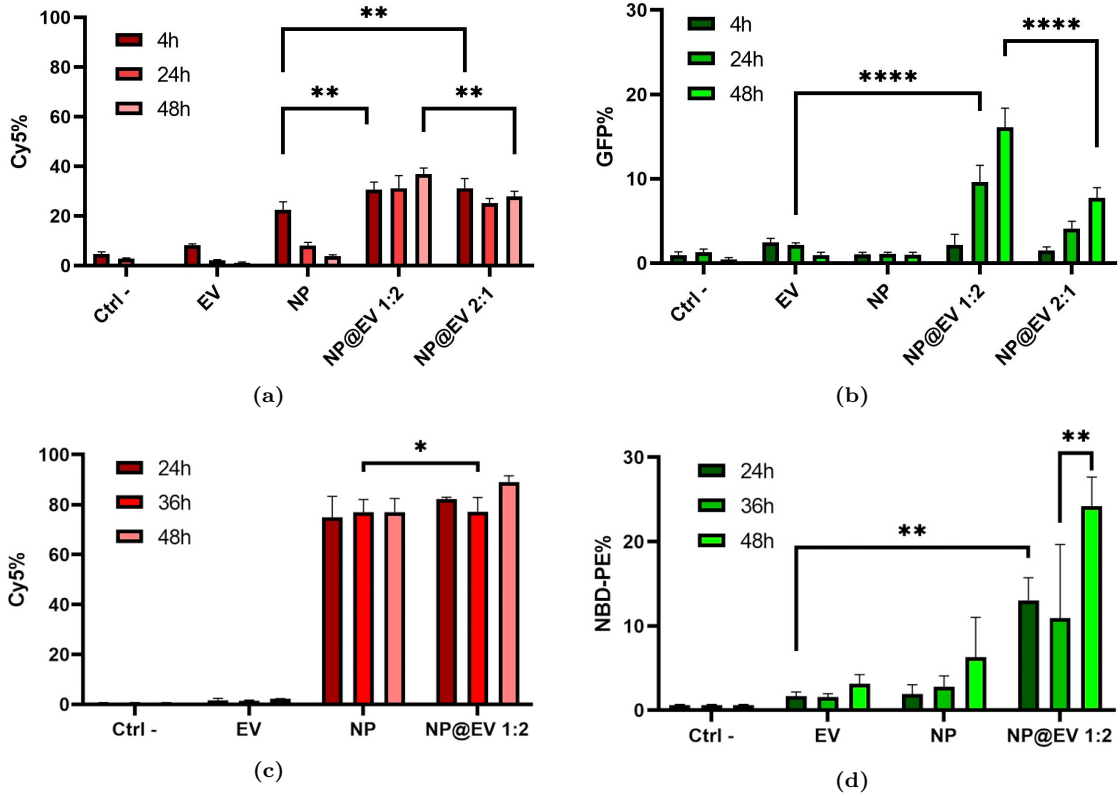


**Figure 4.8:** Internalization assay performed with a flow cytometer using two different lasers to detect Cy5 and GFP/NBD-PE. Percentage of Cy5 (a) and GFP (b) detected in HEK293 at different time points for the negative control group (ctrl-), NP, EV, and different formulations of encapsulated NPs (NP@EV). Percentage of Cy5 (c) and NBD-PE (d) detected in THP1 at different time points for the negative control group (ctrl-), NP, EV, and NP@EV 1:2. On the x-axis are reported the negative control group (Ctrl-) along with the name of the treatments used in each group. *Two-way analysis of variance (ANOVA): \* $p < 0.05$ , \*\* $p < 0.02$ , \*\*\* $p < 0.0001$ .*

Surprisingly EVs alone seem to not enter the cell, while higher signals of GFP can be detected after 24h and 48h in the groups treated with NP@EV. On the other hand, in the formulation NP@EV 2:1 compared to the ratio 1:2 (v/v), a lower GFP signal is observed already after 24 hours. Since the treatment amount was calculated starting from the final concentration of plasmid in each well, NP@EV 2:1 contains only half the total amount of EVs compared to NP@EV 1:2, so lower signals are expected.

For what concern the Cy5 signals, referring to the internalization of the NPs, it is shown a different tendency between the group treated with naked NPs and the groups with the encapsulated one, over time (figure 4.8a). Uptake of encapsulated

NPs is significantly higher already at 4h (around 30%) and remains steady for all of the 48h of the experiment, while naked NPs have a lower internalization percentage (around 20 %) at 4h, and over time the signals lower itself.

Also, between the encapsulated NPs with an excess of EVs (NP@EV 1:2) and the sample with an inverted ratio (NP@EV 2:1) a similar reduction in Cy5 signal can be appreciated at 48h (figure 4.8a). This tendency, already shown by naked NPs, could be another indication that EVs coating changes the kinetics of internalization since the excess of naked NPs in the NP@EV 2:1 sample seems to be cleared faster by the cells.

The time-dependent reduction shown in Figure4.8a could be due to the cell doubling cycle of this cell line (24-36 h) [55], which leads to the clearance of already internalized NPs. For the case of NP@EV 1:2, this destiny does not appear to be shared. This behavior could involve greater stability in the culture medium, granted by coating the EVs. However, this hypothesis should be evaluated in more studies.

The second *in vitro* study was conducted on THP-1 cell line. This cell line represents a model with greater similarity to the real objective of our vaccine. Which is much more restrictive for transfection experiments than HEK-293.

In this experiment, only THP-1 derived-EVs were used, based on the previous experiment in which the sample with an inverted ratio (NP@EV 2:1) achieved less internalization after 24h and 48h. In this case, the absorption of the formulation has been studied with the formulation: NP@EV 1:2.

In Figure 4.8c, 4.8d are reported the percentage of cells positive to the two fluorescent labels used, NBD-PE for EVs and Cy5 for NPs; here we compared the internalization capability of EVs and NPs alone and encapsulated NPs into EVs with a ratio of 1:2 between NPs and EVs, at 24h, 36h, and 48h. Only at 48h a significantly increased signal of Cy5 is detected in the group treated with NP@EV, while high internalization is maintained throughout the experiment.

The previous results agree with what is shown in Figure4.8d, showing that very low levels of EV are internalized when cultured alone to cell culture. The dependence over time was again evidenced where higher levels can be evaluated after 24 h with an increasing percentage throughout 48 h. In this case, the decreasing trend in Cy5% is no longer present in the group treated with naked NPs, this could be due to the longer doubling time of the THP-1 cell line, which is 60-70h [56].

In summary, EV coating appears to increase the internalization of naked NPs and helps maintain a higher level of internalized NPs over time. On the other hand, EVs alone do not show any particular trend in cell internalization. In the case of absorption it is evident from figure 4.8b and 4.8d, that EVs are internalized when combined with NP. The increase in surface charge when EVs coat cationic NPs leads us to believe that strongly negative lipid vesicles have a lower tendency to be internalized by cells, considering the cell membrane charge (negative charges) [7].

### 4.3.2 Confocal microscopy to qualitatively study cell internalization

THP-1 monocytic cells do not express adhesion properties, which makes confocal analysis hard or impossible to achieve with traditional protocols. Instead, we exploit the differentiation capability of the human monocytic leukemia cell line THP-1 to obtain immature dendritic cells (imDCs), which are expected, and have shown later, more adhesion properties allowing the analysis at the confocal microscope. The correct differentiation was then proven by immunofluorescence flow cytometry in order to verify the overexpression of CD86 (figure 4.9), a differentiation marker of imDCs[57].

To further investigate the uptake of encapsulated NPs, imDCs were treated with EVs and NPs alone and NP@EV 1:2, with EVs and NPs labeled as previously explained and the uptake as evaluated at 6h and 48h of treatment through the visualization at the confocal microscope. In Figure 4.10a and figure 4.10b are reported the images from the confocal microscope of respectively the 6h and the 48h treatments. From the control sample emerge a small amount of cross-talk among different dyes, although it is not significant to affect the results. EVs enter for a small amount after 6h as can be evaluated from the microscope, while at 48h no clear EVs signal can be detected. A generally higher intensity in the Cy5 channels (devoted to NPs) can be seen if comparing 6h and 48h samples with the respective negative control (NC), but as for the EVs before seems like only a small amount entered the cell. On the contrary, NP@EV generated stronger signals both at 6h and 48h indicating a higher amount of the nanosystem entered the cell. Although, cell membranes appear damaged in this sample, especially in the 48h treated cells.

These results obtained from the confocal microscope agree with and confirm the flow cytometry data about internalization, underlying a generally increased internalization of both NPs and EVs when they are subjected through our formulation of NP@EV, whether the naked NPs or the EVs alone.

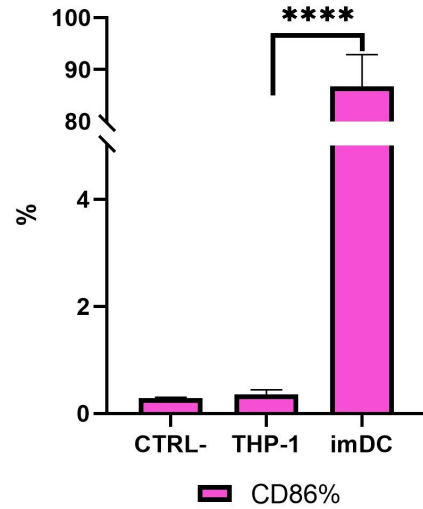
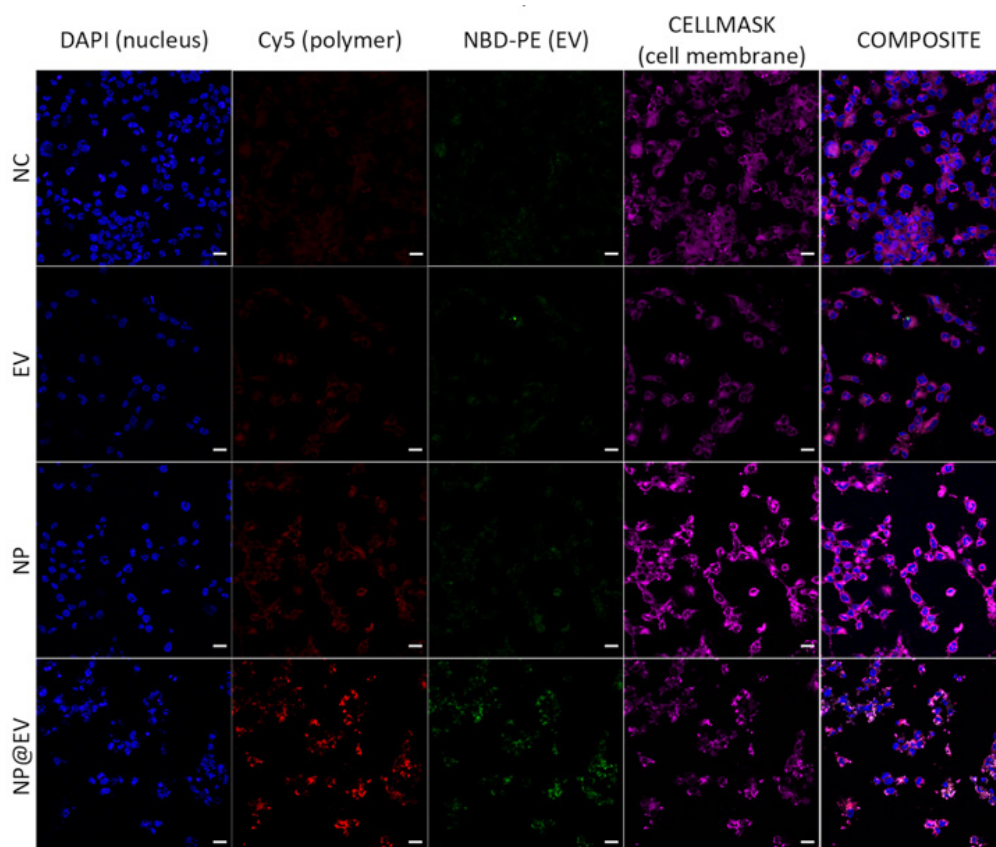
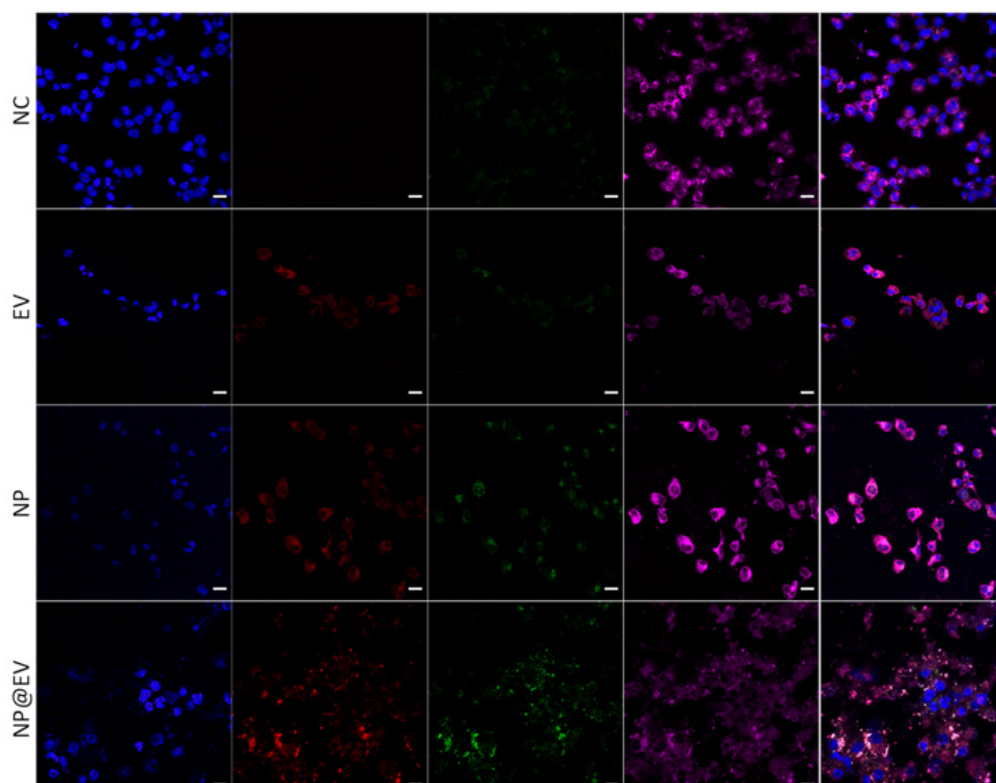


**Figure 4.9:** Immunofluorescence assay of THP-1 and imDC evaluated the expression of CD86 before and after differentiation protocol. Also, a negative control (CTRL-) without conjugated antibody was included. \*\*\*\* $p < 0.0001$



(a)



(b)

**Figure 4.10:** Confocal microscopy of EV, NP, and NP@EV after (a) 6h and (b) 48h of incubation. The sample name is reported on the left-hand side while the fluorophore shown in the channel is written in the top row. Scalebar =  $20\mu m$

# Chapter 5

## Conclusions

The results obtained from the previously explained experiments let us condense some conclusions.

Preliminary studies evaluating the feasibility of the encapsulation methods led to the discarding of both sonication and extrusion methods. pBAEs NPs happened to be too delicate to survive the extrusion process, while only an increased size distribution was observed after sonication, without losing the transfection ability. On the other hand, the evaluation of the effects of repeated freeze-thaw cycles on EVs confirmed the conformational changes and the rearranging of lipid bilayer caused by these thermal processes.

Finally, the application of both freeze-thaw and membrane fusion methods, as explained previously, resulted in what was assumed to be the EV-coated NPs. Size and  $\zeta$ -potential of the encapsulated system respectively, were increased and decreased, congruently to the expectation. The resulting NP@EV were slightly bigger and with negative surface charge, characteristics given by the EV coating. The microscopy images given by two different techniques, confocal microscopy, and hyperspectral microscopy, demonstrated the colocalization of the extracellular vesicles lipid bilayer with the pBAEs NPs. *In vitro* internalization experiments analyzed with flow cytometry and confocal microscopy with fixed cells demonstrated the synergy of this two-compartment system. While EVs alone were not detected inside the cells, the internalization was clear when the EVs were used as coating of the NPs. Moreover, the already high uptake levels of naked NPs were either maintained or increased in two different *in vitro* models.

In conclusion, this proof of concept demonstrated a feasible method to encapsulate pBAEs NPs into EVs, laying the groundwork to build an active targeted drug delivery system capable of delivering the antigen-encoding nucleic acid directly to the antigen-presenting cells, applicable to the production of an anticancer vaccine.

## Chapter 6

# Future steps

The feasibility of the pBAE NPs encapsulation inside EVs is a matter of this thesis; however, further experiments are mandatory in order to assess this method's complete potential. Here interesting experiments that would provide important knowledge are briefly explored:

- CryoTEM of the encapsulated NPs would be necessary to visualize and clear out the morphological features of the system. Moreover, exploiting FRET potential, the encapsulation could be verified with a complementary technique that also provides information about the distance between the lipidic bilayer and the polymers. In this context, a quantitative measure of encapsulation efficiency is also basic information needed when we are investigating encapsulation processes, and this information would be fundamental to further optimize the encapsulation parameters.
- On the other hand, more *in vitro* testing would be necessary. In order to verify the selective cellular uptake, an internalization assay performed on a co-culture model would prove the effective cell targeting feature of the system. Besides, different DC maturation stages provide EVs with different targeting features which could also be evaluated in a comparative study. Last but not least, the use of a model antigen encoding plasmid, such as pOVA, would effectively assess the ultimate transfection efficiency.

# Bibliography

- [1] Sofia Farkona, Eleftherios P. Diamandis, and Ivan M. Blasutig. «Cancer immunotherapy: The beginning of the end of cancer?» In: *BMC Medicine* 14.1 (2016), pp. 1–18. ISSN: 17417015. DOI: [10.1186/s12916-016-0623-5](https://doi.org/10.1186/s12916-016-0623-5). URL: <http://dx.doi.org/10.1186/s12916-016-0623-5> (cit. on pp. 1, 4–6).
- [2] Weiqi Wang, Madiha Saeed, Yao Zhou, Lili Yang, Dange Wang, and Haijun Yu. «Non-viral gene delivery for cancer immunotherapy». In: *Journal of Gene Medicine* 21.7 (2019). ISSN: 15212254. DOI: [10.1002/jgm.3092](https://doi.org/10.1002/jgm.3092) (cit. on pp. 1, 7).
- [3] Nathaly Segovia, Pere Dosta, Anna Cascante, Victor Ramos, and Salvador Borrós. «Oligopeptide-terminated poly( $\beta$ -amino ester)s for highly efficient gene delivery and intracellular localization». In: *Acta Biomaterialia* 10.5 (2014), pp. 2147–2158. ISSN: 18787568. DOI: [10.1016/J.ACTBIO.2013.12.054](https://doi.org/10.1016/J.ACTBIO.2013.12.054) (cit. on pp. 1, 7, 11, 12).
- [4] Pere Dosta, Nathaly Segovia, Anna Cascante, Victor Ramos, and Salvador Borrós. «Surface charge tunability as a powerful strategy to control electrostatic interaction for high efficiency silencing, using tailored oligopeptide-modified poly(beta-amino ester)s (PBAEs)». In: *Acta Biomaterialia* 20 (2015), pp. 82–93. ISSN: 18787568. DOI: [10.1016/j.actbio.2015.03.029](https://doi.org/10.1016/j.actbio.2015.03.029). URL: <http://dx.doi.org/10.1016/j.actbio.2015.03.029> (cit. on pp. 1, 7).
- [5] P. Dosta, V. Ramos, and S. Borrós. «Stable and efficient generation of poly( $\beta$ -amino ester)s for RNAi delivery». In: *Molecular Systems Design and Engineering* 3.4 (2018), pp. 677–689. ISSN: 20589689. DOI: [10.1039/c8me00006a](https://doi.org/10.1039/c8me00006a) (cit. on pp. 1, 7).
- [6] Cristina Fornaguera, Marta Guerra-Rebollo, Miguel Ángel Lázaro, Anna Cascante, Núria Rubio, Jerónimo Blanco, and Salvador Borrós. «In Vivo Retargeting of Poly(beta aminoester) (OM-PBAE) Nanoparticles is Influenced by Protein Corona». In: *Advanced Healthcare Materials* 8.19 (2019), pp. 1–11. ISSN: 21922659. DOI: [10.1002/adhm.201900849](https://doi.org/10.1002/adhm.201900849) (cit. on pp. 1, 7).

- [7] Juewen Liu, Xingmao Jiang, Carlee Ashley, and C. Jeffrey Brinker. «Electrostatically mediated liposome fusion and lipid exchange with a nanoparticle-supported bilayer for control of surface charge, drug containment, and delivery». In: *Journal of the American Chemical Society* 131.22 (2009), pp. 7567–7569. ISSN: 00027863. DOI: [10.1021/ja902039y](https://doi.org/10.1021/ja902039y) (cit. on pp. 1, 10, 23, 31).
- [8] Hidetaka Akita et al. «Multi-layered nanoparticles for penetrating the endosome and nuclear membrane via a step-wise membrane fusion process». In: *Biomaterials* 30.15 (2009), pp. 2940–2949. ISSN: 01429612. DOI: [10.1016/j.biomaterials.2009.02.009](https://doi.org/10.1016/j.biomaterials.2009.02.009). URL: <http://dx.doi.org/10.1016/j.biomaterials.2009.02.009> (cit. on pp. 1, 10, 23).
- [9] Robert J. Lee and Leaf Huang. «Folate-targeted, anionic liposome-entrapped polylysine-condensed DNA for tumor cell-specific gene transfer». In: *Journal of Biological Chemistry* 271.14 (1996), pp. 8481–8487. ISSN: 00219258. DOI: [10.1074/jbc.271.14.8481](https://doi.org/10.1074/jbc.271.14.8481). URL: <http://dx.doi.org/10.1074/jbc.271.14.8481> (cit. on pp. 1, 10, 23).
- [10] Parinaz Fathi, Lang Rao, and Xiaoyuan Chen. «Extracellular vesicle-coated nanoparticles». In: *View* 2.2 (Apr. 2021), p. 20200187. ISSN: 2688-268X. DOI: [10.1002/VIW.20200187](https://doi.org/10.1002/VIW.20200187). URL: <https://onlinelibrary.wiley.com/doi/full/10.1002/VIW.20200187%20https://onlinelibrary.wiley.com/doi/abs/10.1002/VIW.20200187%20https://onlinelibrary.wiley.com/doi/10.1002/VIW.20200187> (cit. on pp. 1, 8, 10, 19, 20).
- [11] Shaobo Ruan, Zachary Greenberg, Xiaoshu Pan, Pei Zhuang, Nina Erwin, and Mei He. «Extracellular Vesicles as an Advanced Delivery Biomaterial for Precision Cancer Immunotherapy». In: *Advanced Healthcare Materials* 11.5 (2022), pp. 1–17. ISSN: 21922659. DOI: [10.1002/adhm.202100650](https://doi.org/10.1002/adhm.202100650) (cit. on p. 2).
- [12] Liubov Frolova and Isaac T.S. Li. «Targeting Capabilities of Native and Bioengineered Extracellular Vesicles for Drug Delivery». In: *Bioengineering* 9.10 (2022). ISSN: 23065354. DOI: [10.3390/bioengineering9100496](https://doi.org/10.3390/bioengineering9100496) (cit. on pp. 2, 8, 9).
- [13] Jacques Ferlay, Murielle Colombet, Isabelle Soerjomataram, Donald M. Parkin, Marion Piñeros, Ariana Znaor, and Freddie Bray. «Cancer statistics for the year 2020: An overview». In: *International Journal of Cancer* 149.4 (2021), pp. 778–789. ISSN: 10970215. DOI: [10.1002/ijc.33588](https://doi.org/10.1002/ijc.33588) (cit. on p. 3).
- [14] Rebecca L. Siegel, Kimberly D. Miller, Nikita Sandeep Wagle, and Ahmedin Jemal. «Cancer statistics, 2023». In: *CA: A Cancer Journal for Clinicians* 73.1 (2023), pp. 17–48. ISSN: 0007-9235. DOI: [10.3322/caac.21763](https://doi.org/10.3322/caac.21763) (cit. on p. 3).

- [15] Douglas Hanahan. «Hallmarks of Cancer: New Dimensions». In: *Cancer Discovery* 12.1 (2022), pp. 31–46. ISSN: 21598290. DOI: [10.1158/2159-8290.CD-21-1059](https://doi.org/10.1158/2159-8290.CD-21-1059) (cit. on p. 3).
- [16] World Health Organization. In: (). URL: <https://www.who.int/news-room/fact-sheets/detail/cancer> (cit. on p. 3).
- [17] Lynda Wyld, Riccardo A. Audisio, and Graeme J. Poston. «The evolution of cancer surgery and future perspectives». In: *Nature Reviews Clinical Oncology* 12.2 (2015), pp. 115–124. ISSN: 17594782. DOI: [10.1038/nrclinonc.2014.191](https://doi.org/10.1038/nrclinonc.2014.191) (cit. on p. 4).
- [18] Bruce A. Chabner and Thomas G. Roberts. «Chemotherapy and the war on cancer». In: *Nature Reviews Cancer* 5.1 (2005), pp. 65–72. ISSN: 1474175X. DOI: [10.1038/nrc1529](https://doi.org/10.1038/nrc1529) (cit. on p. 4).
- [19] Nafiseh Behranvand, Farzad Nasri, Reza Zolfaghari Emameh, Pouria Khani, Asieh Hosseini, Johan Garssen, and Reza Falak. «Chemotherapy: a double-edged sword in cancer treatment». In: *Cancer Immunology, Immunotherapy* 71.3 (2022), pp. 507–526. ISSN: 14320851. DOI: [10.1007/s00262-021-03013-3](https://doi.org/10.1007/s00262-021-03013-3). URL: <https://doi.org/10.1007/s00262-021-03013-3> (cit. on p. 4).
- [20] Helen H.W. Chen and Macus Tien Kuo. «Improving radiotherapy in cancer treatment: Promises and challenges». In: *Oncotarget* 8.37 (2017), pp. 62742–62758. ISSN: 19492553. DOI: [10.18632/oncotarget.18409](https://doi.org/10.18632/oncotarget.18409) (cit. on p. 4).
- [21] Jean Pierre Gillet and Michael M. Gottesman. «Mechanisms of multidrug resistance in cancer.» In: *Methods in molecular biology (Clifton, N.J.)* 596 (2010), pp. 47–76. ISSN: 19406029. DOI: [10.1007/978-1-60761-416-6\\_4](https://doi.org/10.1007/978-1-60761-416-6_4) (cit. on p. 4).
- [22] Coral García-Fernández, Anna Saz, Cristina Fornaguera, and Salvador Borrós. «Cancer immunotherapies revisited: state of the art of conventional treatments and next-generation nanomedicines». In: *Cancer Gene Therapy* 28.9 (2021), pp. 935–946. ISSN: 14765500. DOI: [10.1038/s41417-021-00333-5](https://doi.org/10.1038/s41417-021-00333-5) (cit. on pp. 4–6).
- [23] F. Stephen Hodi et al. «Improved Survival with Ipilimumab in Patients with Metastatic Melanoma». In: *New England Journal of Medicine* 363.8 (2010). PMID: 20525992, pp. 711–723. DOI: [10.1056/NEJMoa1003466](https://doi.org/10.1056/NEJMoa1003466). eprint: <https://doi.org/10.1056/NEJMoa1003466>. URL: <https://doi.org/10.1056/NEJMoa1003466> (cit. on p. 5).
- [24] Carla Giacobino, Marta Canta, Cristina Fornaguera, Salvador Borrós, and Valentina Cauda. «Extracellular vesicles and their current role in cancer immunotherapy». In: *Cancers* 13.9 (2021), pp. 1–24. ISSN: 20726694. DOI: [10.3390/cancers13092280](https://doi.org/10.3390/cancers13092280) (cit. on pp. 5, 6).

- [25] Katsuaki Sato and Shigeharu Fujita. «Dendritic cells-nature and classification». In: *Allergology International* 56.3 (2007), pp. 183–191. ISSN: 14401592. DOI: [10.2332/allergolint.R-06-139](https://doi.org/10.2332/allergolint.R-06-139). URL: <http://dx.doi.org/10.2332/allergolint.R-06-139> (cit. on p. 6).
- [26] John J Suschak, James A Williams, Connie S Schmaljohn, John J Suschak, James A Williams, and Connie S Schmaljohn. «Advancements in DNA vaccine vectors , non- mechanical delivery methods , and molecular adjuvants to increase immunogenicity». In: 5515 (2017). DOI: [10.1080/21645515.2017.1330236](https://doi.org/10.1080/21645515.2017.1330236). URL: <https://doi.org/10.1080/21645515.2017.1330236> (cit. on p. 6).
- [27] Norbert Pardi, Michael J. Hogan, Frederick W. Porter, and Drew Weissman. «mRNA vaccines-a new era in vaccinology». In: *Nature Reviews Drug Discovery* 17.4 (2018), pp. 261–279. ISSN: 14741784. DOI: [10.1038/nrd.2017.243](https://doi.org/10.1038/nrd.2017.243). URL: <http://dx.doi.org/10.1038/nrd.2017.243> (cit. on p. 6).
- [28] Johan Karlsson, Kelly R. Rhodes, Jordan J. Green, and Stephany Y. Tzeng. «Poly(beta-amino ester)s as gene delivery vehicles: challenges and opportunities». In: *Expert Opinion on Drug Delivery* 0.0 (2020). ISSN: 17447593. DOI: [10.1080/17425247.2020.1796628](https://doi.org/10.1080/17425247.2020.1796628). URL: <https://doi.org/10.1080/17425247.2020.1796628> (cit. on pp. 7, 8).
- [29] James I. Andorko, Kevin G. Pineault, and Christopher M. Jewell. «Impact of molecular weight on the intrinsic immunogenic activity of poly(beta amino esters)». In: *Journal of Biomedical Materials Research Part A* 105.4 (2017), pp. 1219–1229. DOI: <https://doi.org/10.1002/jbm.a.35970>. eprint: <https://onlinelibrary.wiley.com/doi/pdf/10.1002/jbm.a.35970>. URL: <https://onlinelibrary.wiley.com/doi/abs/10.1002/jbm.a.35970> (cit. on p. 7).
- [30] Charles H. Jones, Mingfu Chen, Anitha Ravikrishnan, Ryan Reddinger, Guojian Zhang, Anders P. Hakansson, and Blaine A. Pfeifer. «Mannosylated poly(beta-amino esters) for targeted antigen presenting cell immune modulation». In: *Biomaterials* 37 (2015), pp. 333–344. ISSN: 18785905. DOI: [10.1016/j.biomaterials.2014.10.037](https://doi.org/10.1016/j.biomaterials.2014.10.037) (cit. on p. 8).
- [31] Eberhard G. Trams, Carl J. Lauter, Jr Norman Salem, and Ursula Heine. «Exfoliation of membrane ecto-enzymes in the form of micro-vesicles». In: *BBA - Biomembranes* 645.1 (1981), pp. 63–70. ISSN: 00052736. DOI: [10.1016/0005-2736\(81\)90512-5](https://doi.org/10.1016/0005-2736(81)90512-5) (cit. on p. 8).
- [32] Mikołaj P. Zaborowski, Leonora Balaj, Xandra O. Breakefield, and Charles P. Lai. «Extracellular Vesicles: Composition, Biological Relevance, and Methods of Study». In: *BioScience* 65.8 (June 2015), pp. 783–797. ISSN: 0006-3568. DOI: [10.1093/biosci/biv084](https://doi.org/10.1093/biosci/biv084). eprint: <https://academic.oup.com/>

- [bioscience/article-pdf/65/8/783/5041747/biv084.pdf](https://doi.org/10.1093/biosci/biv084). URL: <https://doi.org/10.1093/biosci/biv084> (cit. on p. 8).
- [33] Simona Villata, Marta Canta, and Valentina Cauda. «Evs and bioengineering: From cellular products to engineered nanomachines». In: *International Journal of Molecular Sciences* 21.17 (2020), pp. 1–32. ISSN: 14220067. DOI: [10.3390/ijms21176048](https://doi.org/10.3390/ijms21176048) (cit. on p. 8).
- [34] Jacopo Meldolesi. «Exosomes and Ectosomes in Intercellular Communication». In: *Current Biology* 28.8 (2018), R435–R444. ISSN: 09609822. DOI: [10.1016/j.cub.2018.01.059](https://doi.org/10.1016/j.cub.2018.01.059). URL: <https://doi.org/10.1016/j.cub.2018.01.059> (cit. on p. 8).
- [35] Clotilde Théry et al. «Minimal information for studies of extracellular vesicles 2018 (MISEV2018): a position statement of the International Society for Extracellular Vesicles and update of the MISEV2014 guidelines». In: *Journal of Extracellular Vesicles* 7.1 (2018). ISSN: 20013078. DOI: [10.1080/20013078.2018.1535750](https://doi.org/10.1080/20013078.2018.1535750) (cit. on pp. 8, 28).
- [36] Clotilde Théry, Matias Ostrowski, and Elodie Segura. «Membrane vesicles as conveyors of immune responses». In: *Nature Reviews Immunology* 2009 9:8 9.81. Théry C, Ostrowski M, Segura E. Membrane vesicles as conveyors of immune responses. *Nat Rev Immunol* 2009 9(8):581–593. doi:10.1038/nri2567 (June 2009), pp. 581–593. ISSN: 1474-1741. DOI: [10.1038/nri2567](https://doi.org/10.1038/nri2567). URL: <https://www.nature.com/articles/nri2567> (cit. on p. 9).
- [37] Laura Ann Mulcahy, Ryan Charles Pink, and David Raul Francisco Carter. «Routes and mechanisms of extracellular vesicle uptake». In: *Journal of Extracellular Vesicles* 3.1 (2014). ISSN: 20013078. DOI: [10.3402/JEV.V3.24641](https://doi.org/10.3402/JEV.V3.24641) (cit. on p. 9).
- [38] Kinsley C French, Marc A Antonyak, and Richard A Cerione. «Extracellular vesicle docking at the cellular port: Extracellular vesicle binding and uptake». In: *Seminars in Cell & Developmental Biology* 67 (2017), pp. 48–55. DOI: [10.1016/j.semcdb.2017.01.002](https://doi.org/10.1016/j.semcdb.2017.01.002). URL: <http://dx.doi.org/10.1016/j.semcdb.2017.01.002> (cit. on p. 9).
- [39] María Mittelbrunn, Cristina Gutiérrez-Vázquez, Carolina Villarroja-Beltri, Susana González, Fátima Sánchez-Cabo, Manuel Ángel González, Antonio Bernad, and Francisco Sánchez-Madrid. «Unidirectional transfer of microRNA-loaded exosomes from T cells to antigen-presenting cells». In: *Nature Communications* 2.1 (2011). ISSN: 20411723. DOI: [10.1038/ncomms1285](https://doi.org/10.1038/ncomms1285) (cit. on p. 9).

- [40] Matthew J. Haney et al. «Exosomes as drug delivery vehicles for Parkinson’s disease therapy». In: *Journal of Controlled Release* 207 (2015), pp. 18–30. ISSN: 18734995. DOI: [10.1016/j.jconrel.2015.03.033](https://doi.org/10.1016/j.jconrel.2015.03.033). URL: <http://dx.doi.org/10.1016/j.jconrel.2015.03.033> (cit. on p. 9).
- [41] Myung Soo Kim et al. «Development of exosome-encapsulated paclitaxel to overcome MDR in cancer cells». In: *Nanomedicine: Nanotechnology, Biology, and Medicine* 12.3 (2016), pp. 655–664. ISSN: 15499642. DOI: [10.1016/j.nano.2015.10.012](https://doi.org/10.1016/j.nano.2015.10.012). URL: <http://dx.doi.org/10.1016/j.nano.2015.10.012> (cit. on p. 9).
- [42] Tanziela Tanzuela, Sana Shaikh, Hui Jiang, Zuhong Lu, and Xuemei Wang. «Efficient encapsulation of biocompatible nanoparticles in exosomes for cancer theranostics». In: *Nano Today* 35 (2020), p. 100964. ISSN: 1878044X. DOI: [10.1016/j.nantod.2020.100964](https://doi.org/10.1016/j.nantod.2020.100964). URL: <https://doi.org/10.1016/j.nantod.2020.100964> (cit. on pp. 10, 19).
- [43] Bernhard Illes, Patrick Hirschle, Sabine Barnert, Valentina Cauda, Stefan Wuttke, and Hanna Engelke. «Exosome-coated metal-organic framework nanoparticles: An efficient drug delivery platform». In: *Chemistry of Materials* 29.19 (2017), pp. 8042–8046. ISSN: 15205002. DOI: [10.1021/acs.chemmater.7b02358](https://doi.org/10.1021/acs.chemmater.7b02358) (cit. on pp. 10, 19, 23).
- [44] Cristina Fornaguera et al. «mRNA Delivery System for Targeting Antigen-Presenting Cells In Vivo». In: *Advanced Healthcare Materials* 7.17 (2018), pp. 1–11. ISSN: 21922659. DOI: [10.1002/adhm.201800335](https://doi.org/10.1002/adhm.201800335) (cit. on p. 12).
- [45] Roger Riera, Natalia Feiner-Gracia, Cristina Fornaguera, Anna Cascante, Salvador Borrós, and Lorenzo Albertazzi. «Tracking the DNA complexation state of pBAE polyplexes in cells with super resolution microscopy». In: *Nanoscale* 11.38 (2019), pp. 17869–17877. ISSN: 20403372. DOI: [10.1039/c9nr02858g](https://doi.org/10.1039/c9nr02858g) (cit. on p. 12).
- [46] Mònica Guarro, Francisca Suñer, Martí Lecina, Salvador Borrós, and Cristina Fornaguera. «Efficient extracellular vesicles freeze-dry method for direct formulations preparation and use». In: *Colloids and Surfaces B: Biointerfaces* 218.August (2022). ISSN: 18734367. DOI: [10.1016/j.colsurfb.2022.112745](https://doi.org/10.1016/j.colsurfb.2022.112745) (cit. on p. 13).
- [47] Jörg Stetefeld, Sean A. McKenna, and Trushar R. Patel. «Dynamic light scattering: a practical guide and applications in biomedical sciences». In: *Biophysical Reviews* 8.4 (2016), pp. 409–427. ISSN: 18672469. DOI: [10.1007/s12551-016-0218-6](https://doi.org/10.1007/s12551-016-0218-6). URL: <http://dx.doi.org/10.1007/s12551-016-0218-6> (cit. on p. 14).

- [48] Vasco Filipe, Andrea Hawe, and Wim Jiskoot. «Critical evaluation of nanoparticle tracking analysis (NTA) by NanoSight for the measurement of nanoparticles and protein aggregates». In: *Pharmaceutical Research* 27.5 (2010), pp. 796–810. ISSN: 07248741. DOI: [10.1007/s11095-010-0073-2](https://doi.org/10.1007/s11095-010-0073-2) (cit. on p. 14).
- [49] Prakash Gangadaran and Byeong Cheol Ahn. «Extracellular vesicle-and extracellular vesicle mimetics-based drug delivery systems: New perspectives, challenges, and clinical developments». In: *Pharmaceutics* 12.5 (2020). ISSN: 19994923. DOI: [10.3390/pharmaceutics12050442](https://doi.org/10.3390/pharmaceutics12050442) (cit. on pp. 19, 22, 29).
- [50] Gregor Fuhrmann, Andrea Serio, Manuel Mazo, Rekha Nair, and Molly M. Stevens. «Active loading into extracellular vesicles significantly improves the cellular uptake and photodynamic effect of porphyrins». In: *Journal of Controlled Release* 205 (2015). 3rd Symposium on Innovative Polymers for Controlled Delivery (SIPCD 2014), pp. 35–44. ISSN: 0168-3659. DOI: <https://doi.org/10.1016/j.jconrel.2014.11.029>. URL: <https://www.sciencedirect.com/science/article/pii/S0168365914007779> (cit. on p. 19).
- [51] Che Ming J. Hu, Li Zhang, Santosh Aryal, Connie Cheung, Ronnie H. Fang, and Liangfang Zhang. «Erythrocyte membrane-camouflaged polymeric nanoparticles as a biomimetic delivery platform». In: *Proceedings of the National Academy of Sciences of the United States of America* 108.27 (2011), pp. 10980–10985. ISSN: 00278424. DOI: [10.1073/pnas.1106634108](https://doi.org/10.1073/pnas.1106634108) (cit. on p. 20).
- [52] Feng Gao, Lulu Xu, Binqian Yang, Feng Fan, and Lihua Yang. *Kill the Real with the Fake: Eliminate Intracellular Staphylococcus aureus Using Nanoparticle Coated with Its Extracellular Vesicle Membrane as Active-Targeting Drug Carrier*. 2019. DOI: [10.1021/acsinfecdis.8b00212](https://doi.org/10.1021/acsinfecdis.8b00212) (cit. on p. 20).
- [53] Ruby I. MacDonald and Robert C. MacDonald. «Lipid mixing during freeze-thawing of liposomal membranes as monitored by fluorescence energy transfer». In: *BBA - Biomembranes* 735.2 (1983), pp. 243–251. ISSN: 00052736. DOI: [10.1016/0005-2736\(83\)90299-7](https://doi.org/10.1016/0005-2736(83)90299-7) (cit. on p. 22).
- [54] S. Bolte and F.P. Cordelières. «A guided tour into subcellular colocalization analysis in light microscopy». In: *Journal of Microscopy* 224.June (2006), pp. 213–232 (cit. on p. 26).
- [55] Philip Thomas and Trevor G. Smart. «HEK293 cell line: A vehicle for the expression of recombinant proteins». In: *Journal of Pharmacological and Toxicological Methods* 51.3 SPEC. ISS. (2005), pp. 187–200. ISSN: 10568719. DOI: [10.1016/j.vascn.2004.08.014](https://doi.org/10.1016/j.vascn.2004.08.014) (cit. on p. 31).

- [56] Shigeru Tsuchiya, Michiko Yamabe, Yoshiko Yamaguchi, Yasuko Kobayashi, Tasuke Konno, and Keiya Tada. «Establishment and characterization of a human acute monocytic leukemia cell line (THP-1). *Int J Cancer*. 1980; 26:171–176. DOI: [10.1002/ijc.2910260208](https://doi.org/10.1002/ijc.2910260208)». In: *International Journal of Cancer* 176.2 (1980), pp. 171–176 (cit. on p. 31).
- [57] L. Czernek, A. Chworos, and M. Duechler. *The Uptake of Extracellular Vesicles is Affected by the Differentiation Status of Myeloid Cells*. 2015. DOI: [10.1111/sji.12371](https://doi.org/10.1111/sji.12371) (cit. on p. 32).

# Appendix A

## Supporting information

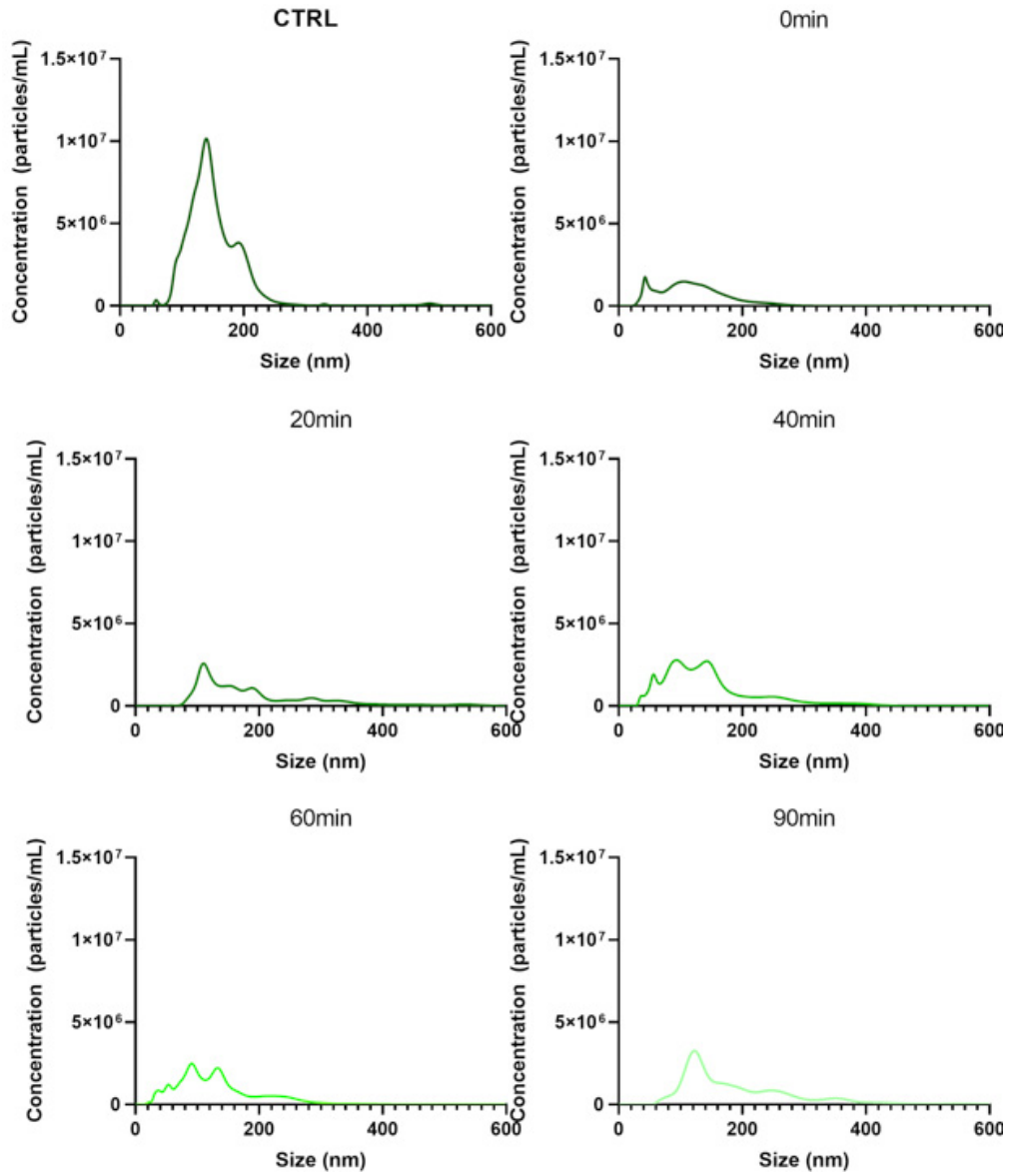


**Figure A.1:** NTA size distribution graphs for EVs before (CTRL) *freeze-thaw* and after different recovering times (0, 20, 40, 60, 90 min)

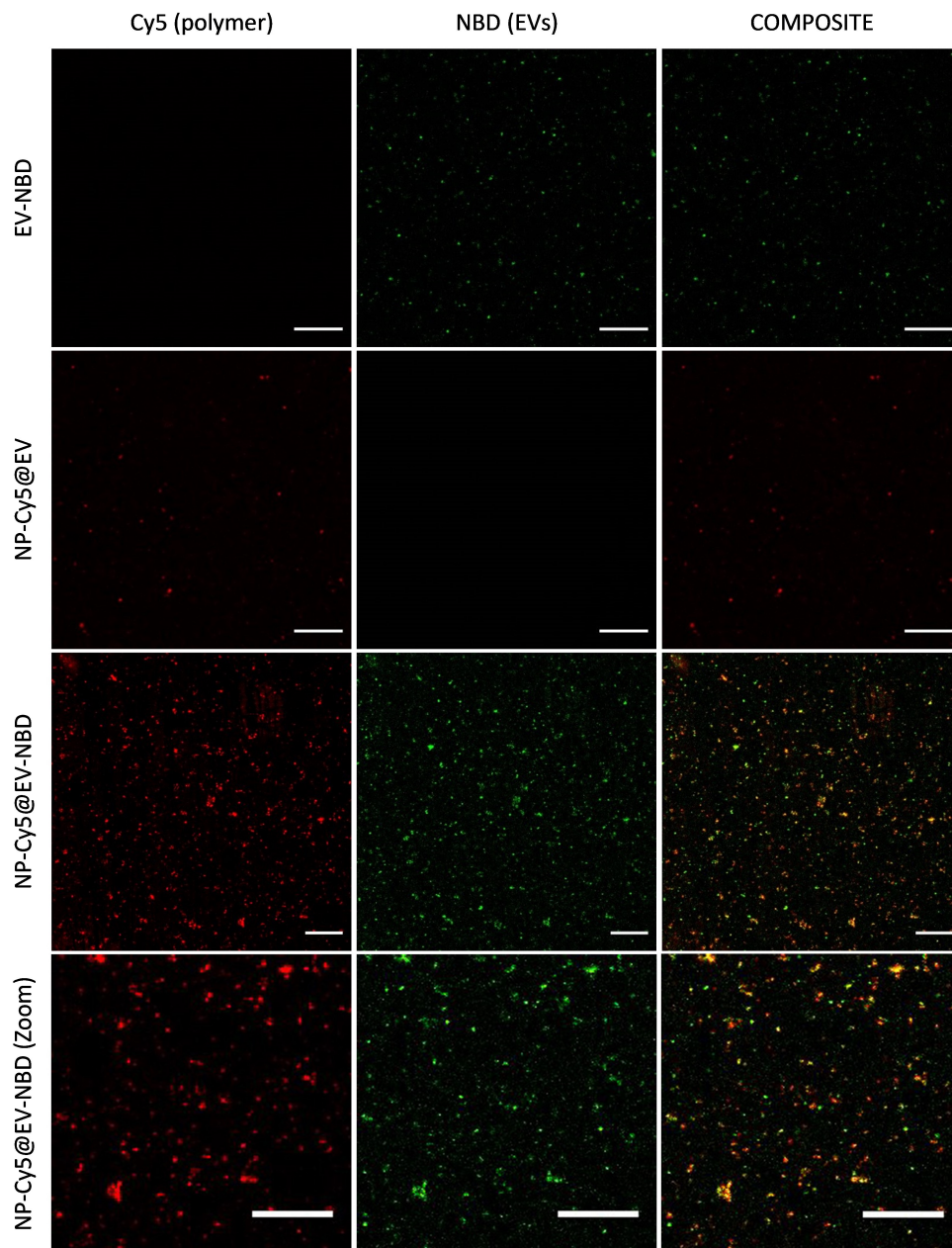


**Figure A.2:** Confocal microscopy of fluorescent labeled EVs and NPs are here reported, including the controls we used to ascertain no cross-signaling was present. Channel name is reported above, while sample name is shown in the right hand side. scalebar =  $10\mu m$

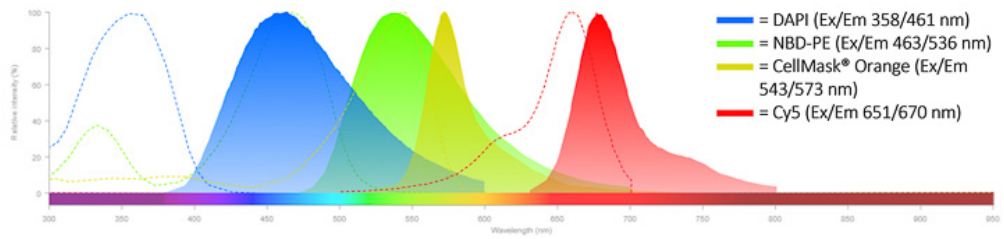


**Figure A.3:** Excitation (dotted line) and emission (continuous line) graphs of fluorophores used to visualize through confocal microscopy the internalization of NPs and EVs into imDCs.